UNIVERSITY OF AMSTERDAM

MASTER THESIS

Rebuilding a Potassium Quantum Gas Apparatus

Author:
Namrata Dutta Mazumdar
Student ID: 10860428

Supervisor:
Prof. Dr. Florian Schreck

Daily Supervisor:
Dr. Benjamin Pasquiou

Second Supervisor:
Dr. Robert Spreeuw

September 2015 - August 2016

60 *ECTS*

A thesis submitted in partial fulfillment of the requirements for the degree of MSc. Physics

Work performed in the group of

Quantum Gases and Quantum Information
Van der Waals-Zeeman Institute
Institute of Physics

August 13, 2016



"To my parents."

Namrata Dutta Mazumdar

UNIVERSITY OF AMSTERDAM

Abstract

Van der Waals-Zeeman Institute
Institute of Physics

MSc. Physics

Rebuilding a Potassium Quantum Gas Apparatus

by Namrata Dutta Mazumdar

This project comprises rebuilding a potassium quantum gas apparatus. The apparatus was originally built and operated in the group of Prof. Dr. Jook Walraven [1]. After Dr. Walraven retired, the apparatus was largely dismantled until Prof. Dr. Florian Schreck inherited it in 2014. Since then a master student was able to achieve a three-dimensional Magneto-Optical Trap (MOT) by building the optical setup around the already existing vacuum setup [2]. After that I have worked on rebuilding, optimising and stabilising the optical setup which will be useful for future generation of experiments with the apparatus.

Acknowledgements

I would like to thank Florian, for being such an enthusiastic teacher and making the lectures so interactive. His enthusiasm is very infectious and made me extremely motivated to pursue this project. Also, his careful comments and corrections were very useful to write this thesis. I have learned a lot from him.

I would like to thank Benjamin, for being extremely critical in the lab. Otherwise, I would not have learned the importance of a stable experimental setup. I have learned a lot of experimental subtleties from him.

I would like to thank the SrPAL and Srμscope team for always letting me borrow their equipments and having the Pandora Box filled with refreshments. I have received a lot of useful experimental tips from ChunChia and Shyane.

I would like to thank the RbSr team for also letting me borrow their equipments. It was nice to have some interesting discussions about science.

I would like to thank Dr. Robert Spreeuw for being my second supervisor at such a short notice.

Finally, I would like to thank my parents for being supportive and motivating me to pursue a career in physics. Thanks to Stephen, for sharing all the happiness and stress during the project!

Contents

Abstract **iii**

Acknowledgements **v**

1 Introduction **1**
1.1 Aim . . . 1
1.2 What are Bose and Fermi Condensates? . . . 1
1.3 Motivation . . . 1
1.4 Overview of this Thesis . . . 2

2 Properties of Potassium **3**
2.1 Atomic Structure of Potassium . . . 3
2.2 Optical Properties of Potassium . . . 5

3 Computer Control **9**
3.1 Radio Frequency Generation . . . 9
3.1.1 Technical Specifications . . . 11
3.1.2 Calibrations . . . 11
3.2 Computer Control of MOT Coils . . . 11
3.3 Computer Control of Shutters . . . 13

4 Master Laser **17**
4.1 Theory of External Cavity Diode Lasers (ECDL) . . . 17
4.2 Technical Specifications . . . 18
4.3 Aligning the Master Laser . . . 19
4.4 Experimental Insights . . . 19

5 Laser Lock Setup **21**
5.1 Doppler-Free Spectroscopy . . . 21
5.2 DAVLL Spectroscopy . . . 22
5.3 Optical Setup and Electronics . . . 23
5.4 Measurements and Results . . . 24
5.4.1 Laser Characteristics . . . 24
5.4.2 Spectroscopy AOM Characteristics . . . 25
5.4.3 Spectroscopy Cell Characteristics . . . 25
5.4.4 Laser Lock Characteristics . . . 26
5.4.5 Knife-Edge Measurement . . . 26
5.4.6 Beam Intensity Calculations . . . 27
5.4.7 Simulations . . . 28

6 Amplifier Setup **33**
6.1 Tapered Amplifiers . . . 33
6.2 Acousto-Optic Modulators . . . 34
6.3 Optical Fibres . . . 35

6.4 Experimental Insights 36
6.5 Measurements 39

7 MOT Setup **41**
7.1 Laser Cooling and Trapping 41
7.1.1 Optical Molasses 41
7.1.2 Magneto-Optical Trap 42
7.2 Vacuum System 43
7.3 Optical Setup 45
7.3.1 2D MOT 45
7.3.2 3D MOT 46
7.4 Fluorescence Imaging 46
7.4.1 Calibrations 47
7.5 Absorption Imaging 48
7.5.1 Mathematical Description 48
7.5.2 Optical setup 49

8 Summary and Outlook **51**
8.1 Summary 51
8.2 Outlook 51

Bibliography **53**

A Computer Code **55**

Chapter 1

Introduction

1.1 Aim

Our lab aims at producing quantum degenerate gases of fermionic potassium atoms using laser cooling and trapping. The first step consists of confining atoms in a small volume and simultaneously laser cooling them down to a few tens of micro-Kelvin, which is popularly known as the 'ultracold regime' [3, 4].This first stage of cooling and trapping is usually achieved by using a Magneto-Optical Trap (MOT), a combination of a magnetic quadrupole field and six orthogonal laser beams [3, 4]. I will be explaining the MOT in detail in Chapter 7.

1.2 What are Bose and Fermi Condensates?

As we cool down the atomic gas to a few milli-Kelvins, the quantum nature of the atoms starts becoming increasingly important, characterized by the size of the atomic wave-packets (de-Broglie wavelength) [4]. Further cooling of the atoms down to ultracold regime, such that the de-Broglie wavelength is larger than the mean inter-particle distance leads to a different state of matter. If the gas consists of identical bosons, all atoms will occupy the same quantum state, which can be described by a single wave-function. This state is known as a Bose-Einstein condensate [3, 4]. If the gas consists of identical fermions, a condensate will not be formed because of the Pauli exclusion principle [5, 6]. It is possible to form a Fermi condensate, by pairing distinguishable fermions into molecules or Cooper pairs, which are bosons and can be Bose condensed [5].

1.3 Motivation

Our main motivation for cooling the atoms is to study quantum many-body physics. We know many examples of many-body physics from nature, for example a swarm of birds. Figure 1.1 depicts the flight patterns of a swarm of birds. There is no 'master-bird' controlling the flight of all other birds, instead the flight patterns emerge from interactions between neighbouring birds and air-currents. Similarly, such emergent phenomena occur from interactions between electrons in solid-state materials. These phenomena lie in the heart of condensed matter physics, which we want to understand [4]. Such emergent phenomena are difficult to predict even if all the details of the microscopic system are known. In order to gain insights, we use well-controlled systems, in our case ultracold atoms to simulate the behaviour of such complicated materials [15]. We precisely control confinement, interactions and internal state of the atoms, thus mimicking the electrons in solid-state materials [4].



FIGURE 1.1: Swam of birds [16].

1.4 Overview of this Thesis

During my thesis I re-built the laser system required for the MOT. The experimental setup consists of five building blocks. First, the computer control system for controlling the whole experiment, including radio-frequency generation for operating the acousto-optic modulators (AOMs); second, the master laser; third, the laser lock setup for stabilizing the laser frequency on a particular atomic transition; fourth, optical setup for amplifying the laser power and shifting its frequency for trapping the atoms; fifth, the MOT setup. I will be explaining these blocks in chapters 3-7.

Chapter 2

Properties of Potassium

In this chapter the atomic structure of potassium (section 2.1) and its interaction with light fields (section 2.2) will be described. These properties form the basis for developing the technology for trapping and cooling potassium atoms. Potassium is an alkali element with one electron in the outermost orbit, making it a highly electropositive and reactive element [8]. Figure 2.1 depicts the position of potassium in the periodic table. Natural potassium is a mixture of two bosonic and one fermionic isotope. Their properties are summarized below in table 2.1 [8]. In our experiment we mainly use two isotopes, namely ^{39}K and ^{40}K.

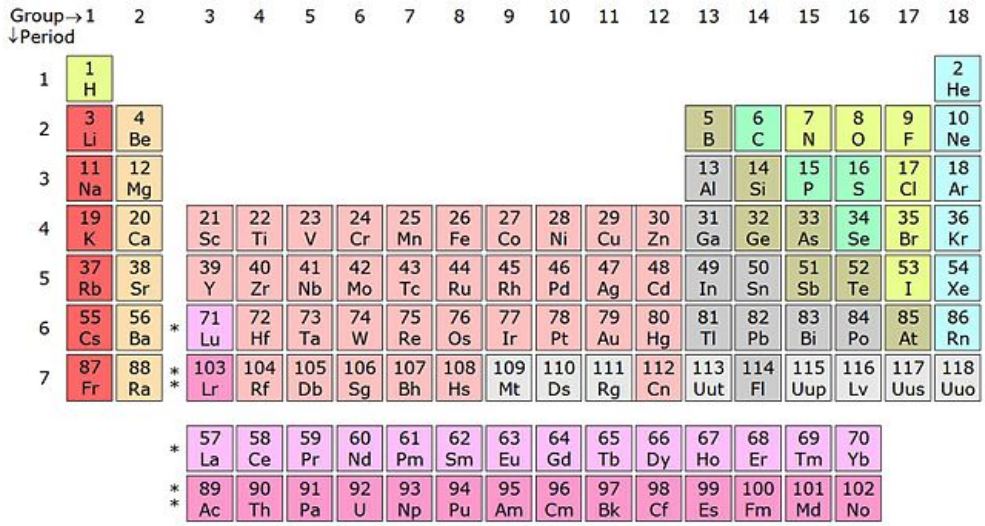


FIGURE 2.1: Potassium is located in Group 1 and Period 4 of the Periodic Table [18].

Mass number	Neutrons	Abundance (%)	Mass (u)	Lifetime	Nuclear spin
39	20	93.25	38.963706	stable	3/2
40	21	0.012	39.963998	1.28 x 10^9 y	4
41	22	6.73	40.961826	stable	3/2

TABLE 2.1: Properties of potassium isotopes [8].

2.1 Atomic Structure of Potassium

In this section physics of the potassium level schemes, as depicted in figure 2.2 will be explained. To begin with, the largest separation between energy levels comes from the

quantization of electron levels in the Coulomb field of the nucleus. The energy of these levels is given by

$$E_n \propto -\frac{Z^2}{n^2}, \tag{2.1}$$

where Z is the number of protons in the atom and n is the principal quantum number. These levels are called electronic energy levels [6]. Subsequently, these electronic levels split into sub-levels, forming the fine structure level scheme. This level scheme arises mainly due to two phenomena. Firstly the mass effect [6], which is caused by the relativistic correction on the mass of the electron for different angular momenta l. The energy shift caused by the mass effect is given by,

$$\Delta E_{\text{mass}} = -E_n \frac{\alpha^2 Z^2}{n^2}\left(\frac{3}{4} - \frac{n}{l+1/2}\right), \tag{2.2}$$

where α is the fine structure constant. The second phenomenon is spin-orbit coupling [6], which arises due to the interaction between the spin of the electron and the magnetic field generated by motion of the electron in its orbit, around the nucleus. The energy shifts due to spin-orbit coupling are

$$\Delta E_{\text{LS}} = \frac{\alpha^2}{nl(l+1)} E(n). \tag{2.3}$$

The total fine structure splitting is then given by

$$\Delta E_{\text{fine}} = \Delta E_{\text{mass}} + \Delta E_{\text{LS}}. \tag{2.4}$$

Finally, the fine structure levels split into hyperfine levels, which arises due to interaction between the electronic magnetic moment and the nuclear magnetic moment I. The corresponding level shifts are given by

$$\Delta E_{\text{hf}} = \frac{\alpha_{\text{hf}}}{2}(I + \frac{1}{2}), \tag{2.5}$$

where α_{hf} is the hyperfine coupling constant [6]. The values of this constant is given in table 2.2.

Constant	Value ^{39}K	Value ^{40}K
α_{hf} for the $^2S_{1/2}$ state	230.859860 MHz$\times h$	-285.73 MHz$\times h$
α_{hf} for the $^2P_{3/2}$ state	6.1 MHz$\times h$	-7.6 MHz$\times h$
g_I	-0.000141935	+0.000176490

TABLE 2.2: Hyperfine structure constants for potassium isotopes [8].

In presence of an external magnetic field, the levels are further split into Zeeman sublevels [6]. Hyperfine and Zeeman shifts are together given by

$$E_{hf}(B) = -\frac{\alpha_{hf}}{4} + g_I \mu_B m_f B \pm \frac{\alpha_{hf}(I+1/2)}{2}\left(1 + \frac{4m_f x}{2I+1} + x^2\right)^{1/2}, \tag{2.6}$$

where m is the magnetic quantum number, $x = \frac{(g_s - g_i)\mu_B}{\alpha_{hf}(I+1.2)} B$, μ_B the Bohr Magnetron and g the Landé g-factor. The different values of g is give in table 2.3.

Constant	Value
g_s	2.00231930436
g_J for the $^2S_{1/2}$ state	2.002294
g_J for the $^2P_{3/2}$ state	4/3

TABLE 2.3: Landé g-factor for potassium states [8].

2.2 Optical Properties of Potassium

In this section the interaction of light fields with potassium atoms will be described. In our experiments we use the D2 transition for laser cooling, as shown in figure 2.2. This transition can be characterized by several parameters, as given in table 2.4 and 2.5.

Property	Symbol	Value
Frequency	ν	391.016170 THz
Wavelength	λ	766.7009218 nm
Wavenumber	$k/2\pi$	13042.895496 cm^{-1}
Lifetime	τ	26.4 ns
Natural linewidth	$\Gamma/2\pi$	6.04 MHz
Recoil velocity	v_{rec}	1.33573614 cm/s
Saturation intensity	I_s	1.75 $\mathrm{mW/cm}^2$

TABLE 2.4: Optical properties of ^{39}K [8].

Property	Symbol	Value
Frequency	ν	391.0162960 THz
Wavelength	λ	766.700675 nm
Wavenumber	$k/2\pi$	13042.89970 cm^{-1}
Lifetime	τ	26.4 ns
Natural linewidth	$\Gamma/2\pi$	6.04 MHz
Recoil velocity	v_{rec}	1.30230332 cm/s
Saturation intensity	I_s	1.75 $\mathrm{W/cm}^2$

TABLE 2.5: Optical properties of ^{40}K [8].

The natural lifetime (τ) of an excited state is related to the natural linewidth (Γ) of the atomic transition by

$$\tau = 1/\Gamma. \tag{2.7}$$

Further, Γ can also be related to a temperature given by

$$k_{\mathrm{B}} T_{\mathrm{D}} = \hbar\Gamma/2, \tag{2.8}$$

which is known as the Doppler Temperature (T_{D}) and k_{B} is the Boltzmann constant. The wavenumber (k), frequency (ν) and wavelength (λ) are related by

$$k = 2\pi/\lambda \tag{2.9}$$

and

$$\nu = c/\lambda, \tag{2.10}$$

where c is the speed of light in vacuum. When an atom of mass (m) emits or absorbs a photon the magnitude of momentum (p) transferred between them is given by

$$p = \hbar k = m v_{\mathrm{rec}}, \tag{2.11}$$

where h is the Planck's constant and $\hbar = \frac{h}{2\pi}$; v_{rec} is the recoil velocity. The final parameter of interest is the saturation intensity of an atom (I_{sat}) given by

$$I_{\mathrm{sat}} = \frac{\pi h c}{3\lambda^3 \tau}. \tag{2.12}$$

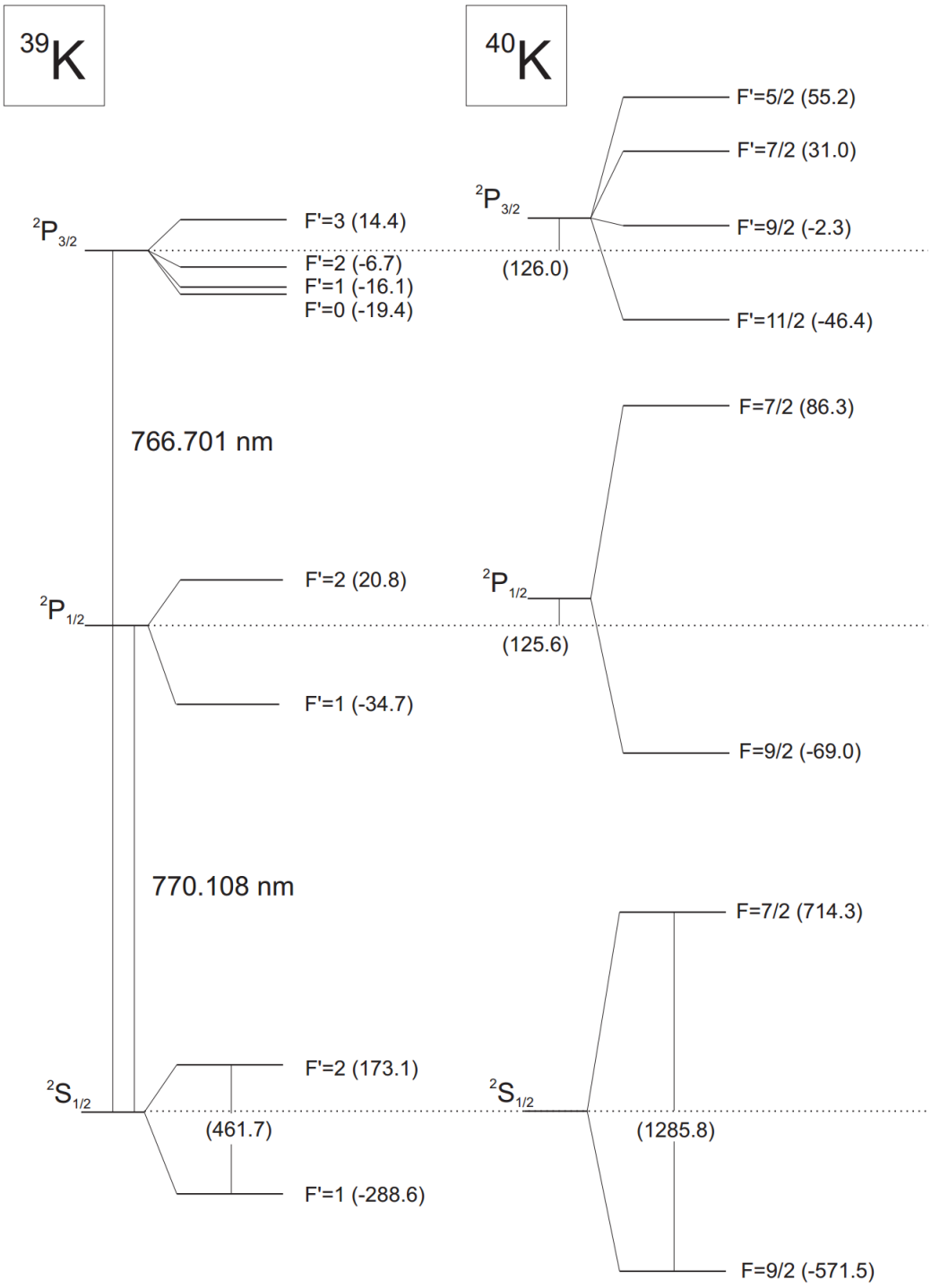


FIGURE 2.2: Level structure of potassium. The S and P states are the fine structure states, whereas the F states are the hyperfine states. The $^2S_{1/2} \rightarrow {}^2P_{1/2}$ and the $^2S_{1/2} \rightarrow {}^2P_{3/2}$ are the $D1$ and $D2$ transitions respectively [2]. The laser is locked on $^2S_{1/2}$, $F^{'}=1 \rightarrow {}^2P_{3/2}$ transition of ^{39}K.

Chapter 3

Computer Control

The computer control system used in the experiment had been developed by Florian Schreck and Todd Meyrath [9].The system is based on a parallel bus which distributes data from a central computer to analog and digital output boards. The bus signals are emitted by a National Instruments (NI) digital output card. Figure 3.1 illustrates a schematic of the computer control along with pictures of NI cards and digital as well as analog output boxes. The control program is written in Visual C++/Borland C++. During this thesis the control system has been modified to suit the needs of the experiments. Figure 3.2 illustrates the user interface for the control software.

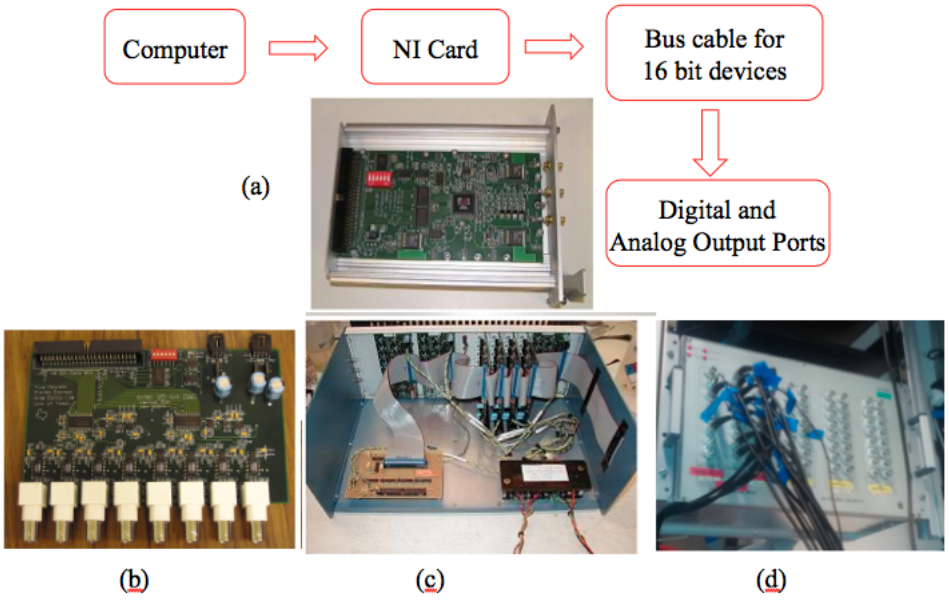


FIGURE 3.1: (a) and (b) are the NI cards used for the experiment; (c) and (d) are the digital and analog output boxes [9].

3.1 Radio Frequency Generation

We need radio-frequency (RF) signals to operate the AOMs. The two experimental parameters we are interested in controlling with the AOMs is the frequency and intensity of the laser beam. Figure 3.3 shows the schematic and a photo of the electronics used for achieving this goal.

The voltage controlled oscillator (VCO) receives a voltage signal from the analog output port and correspondingly releases a signal of a particular frequency. Next the voltage controlled attenuator (VCA) receives the signal from VCO, and attenuates its

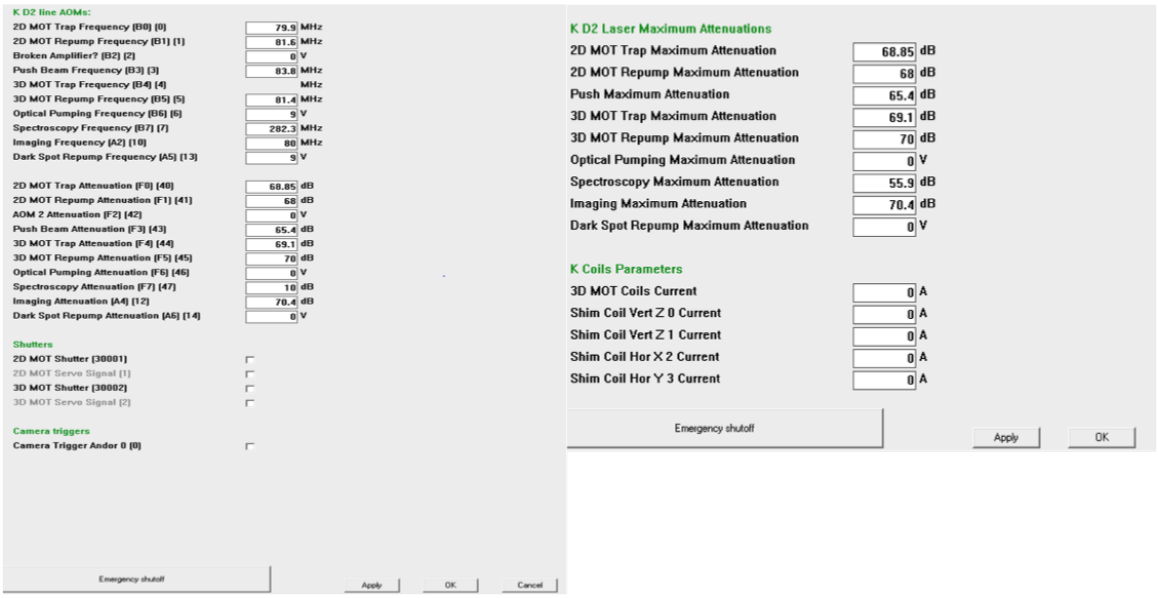


FIGURE 3.2: User interface of the control software. It shows the frequency and attenuation of the AOMs; the shutter control and the camera triggers; and the MOT coils currents.

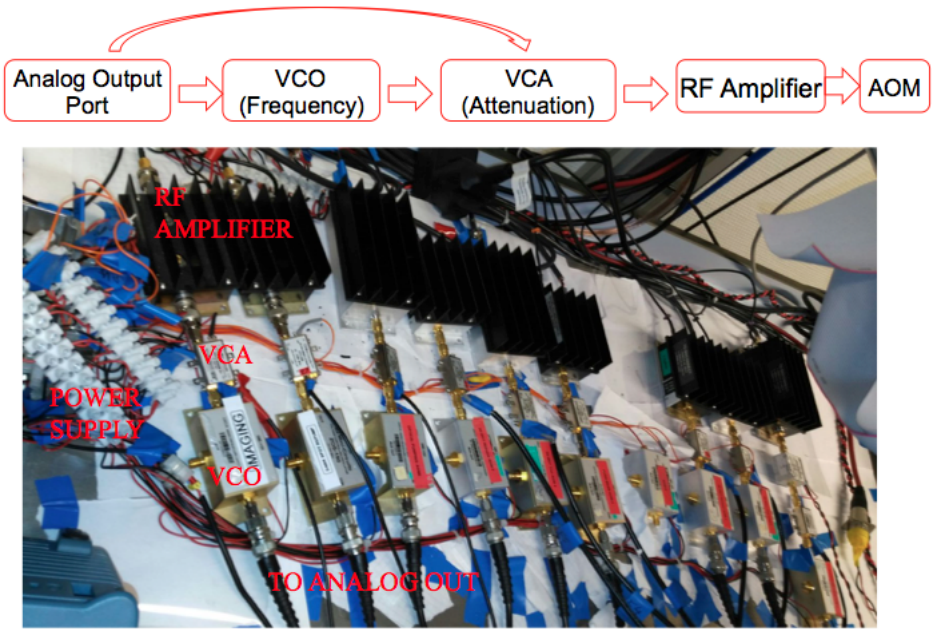


FIGURE 3.3: Schematic of RF Generation with a photo of the electronics used.

power depending on a separate voltage signal received from another analog output port. Finally, the signal from the VCA goes into the RF amplifier, in order to obtain enough power to operate an AOM, about 1 W.

3.1.1 Technical Specifications

The VCOs used are in the range of 50 to 284 MHz, namely (mini-circuits ZOS-100, ZOS-150 and ZOS-300). The VCAs can attenuate in the range of 3 to 70 dB, called (mini-circuits ZX73-2500). The RF- amplifiers are (mini-circuits ZHL-2 and ZHL-3A) which can deliver around 1 W of power, this is sufficient for driving the AOMs. The ZOS-300 VCO has a pre-amplifier attached to its output (mini-circuits ZFL-500LN) in order to provide enough power to drive the main amplifier (ZHL-3A), which in turn provides the required power for the AOM. One of our AOMs requires a RF signal in the microwave regime (1.2435 GHz) that cannot be generated using the available VCOs, thus an external signal generator (Rhode Schwarz SMB100) was used. This device gives us both precise control over the frequency and power.

During this thesis three new sets of VCO, VCA and RF-amplifiers were installed and some broken amplifiers and cables were repaired or replaced. Our RF amplifiers break if their output is not terminated by a 50Ω load, because of all their output power being back-reflected into them. Therefore it is extremely important to always connect a load that is capable of absorbing the RF signal to the amplifier. Special attention needs to paid for matching the RF frequency produced to the frequency bandwidth of a given AOM. Also, a broken cable is equivalent to no load being attached to the amplifier.

3.1.2 Calibrations

During this thesis, the VCOs were calibrated by measuring the frequencies corresponding to the analog voltages using a spectrum analyzer. The calibrations were then incorporated into the control program. The frequencies have been calibrated to a precision of 0.2 MHz around the region of interest. Figure 3.4 shows the frequency calibration curves for all the VCOs. These curves were fitted with polynomial functions using Origin software, which were put into the control program for calibration. Figure A.1 shows an excerpt of the frequency calibration code.

Similarly, the VCAs were calibrated by measuring the attenuation corresponding to the analog voltages. Attenuation is calculated by measuring the output power of the VCO followed by a measurement of the ouput power of the VCA and then dividing these two values by each other (or subtracting them if they are given in the logarithmic dBm scale). After that linear interpolation of the voltage values were done in the given attenuation range using Origin software. Finally, these values were incorporated into the control program and it was programmed suitably for calibration. Figure A.2 shows an excerpt of the calibration code.

3.2 Computer Control of MOT Coils

The current through the MOT coils is provided by a power supply (Delta Elektronika SM15-200D). The current of this power supply is set by a voltage signal from an analog output of the computer control system. The power supply is current programmed and it can be controlled between 0 and 200 A. In order to prevent ground loops and have isolated programming of the coils, analog optical isolator (Delta Elektronika ISO AMP module) is inserted between the analog output and the current control input of the power supply. Figure 3.5 provides a pin-out diagram of the power supply. The analog optical isolator also has a similar pin-out structure. The resistance of the MOT coil was measured to be 26 mΩ. Hence, the power consumed for 10 A of current is only 0.1 W. Figure A.3 provides an excerpt of the calibration code for the power supplies. The user needs to enter the required current from the power supply as input and accordingly the

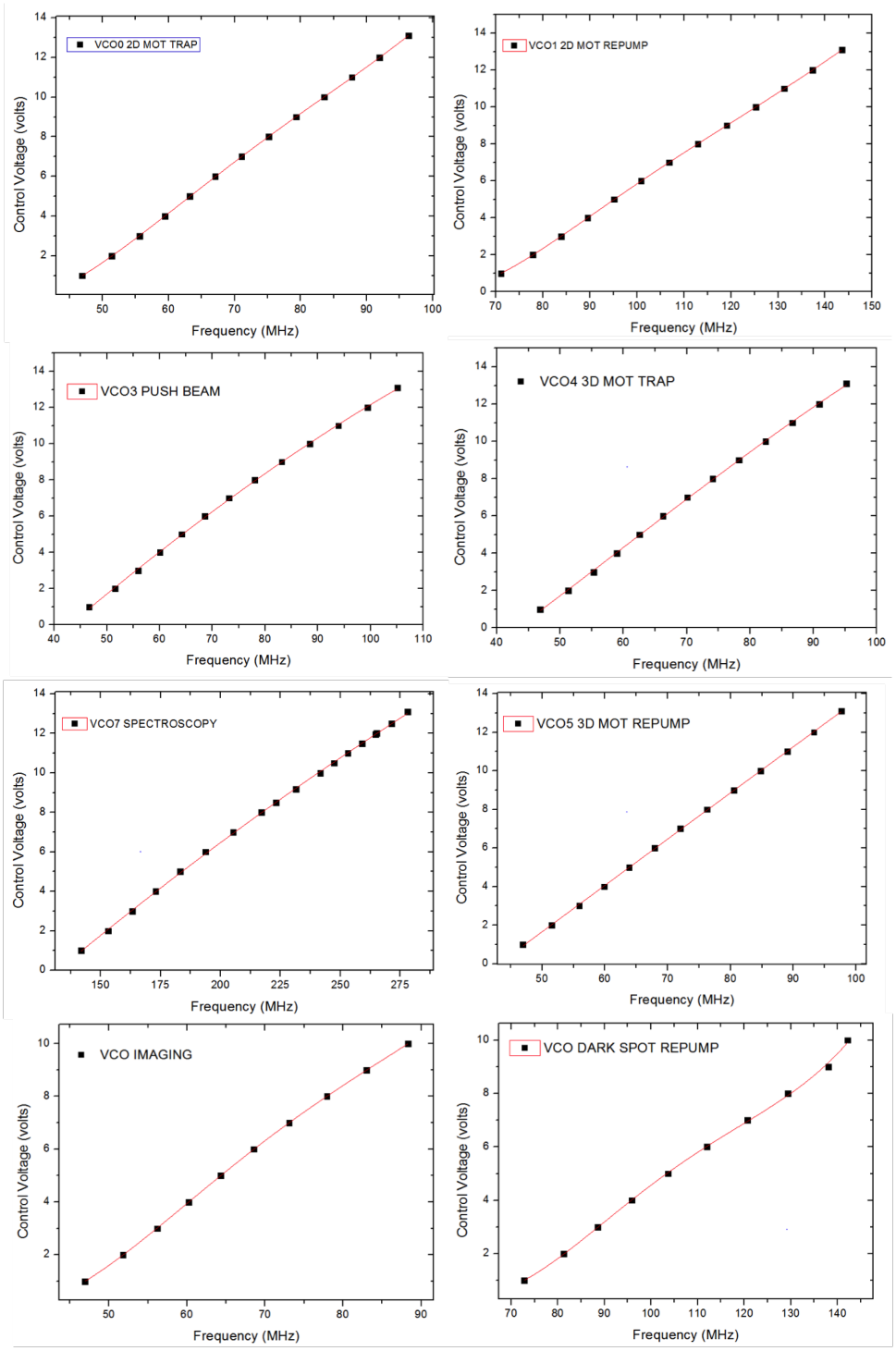


FIGURE 3.4: Frequency calibration curves.

code calibrates the analog output voltage, which is sent to the current programming input of the power supply for giving the required output current.

The MOT coils need to be protected from being damaged by excessively high current. If the current is too high the coils start to overheat and get damaged. Thermal switches have been attached to the coils for opening the interlock of the power supply, interrupting current flow and preventing damage. A small circuit was designed to implement this interlock, see figure 3.6. In the circuit three thermal switches have been

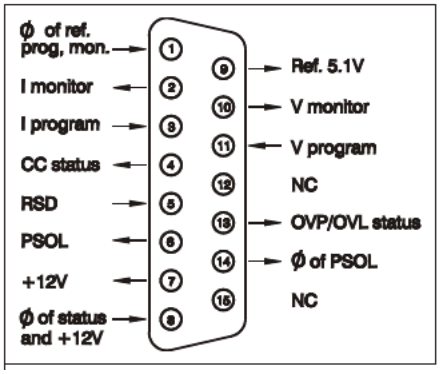


FIGURE 3.5: Pinout diagram of SM15-200D power supply [24].

placed on the current carrying wire, one near to the power supply, and two near the MOT chamber. These switches open above $60°$C. We would like the power supply to shut off in case a thermal switch opens or the cable connecting the thermal switches is inadvertently interrupted. The remote shut down input (RSD), pin 5 of the power supply connector, shuts the power supply down if it receives 5V. We connect RSD to V_{ref} (pin 9), which provides $5.1V$, through three thermal switches connected in series and a TTL NOT-gate, see figure 3.7. The transistor gate (BC549C) is driven by a 5V signal [1]. As long as the switches are below $60°$C the power supply is enabled. If they are heated above that threshold temperature or if the cable connecting the switches is broken, the power supply switches off.

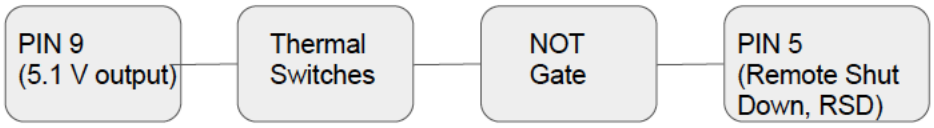


FIGURE 3.6: Interlock circuit.

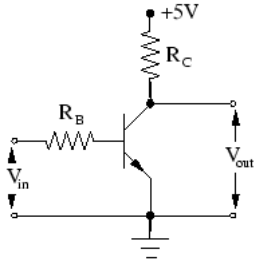


FIGURE 3.7: NOT Gate with a Transistor [17]; $V_{\mathrm{Out}} = -V_{\mathrm{In}}$, R_{B}=10 kΩ and R_{C}=200Ω.

3.3 Computer Control of Shutters

Shutters are used for blocking our laser beams. They are used because they have a much higher attenuation than an AOM, thus effectively blocking the non-diffracted

[1] The 5 V needed for this circuit was derived from the 15 V source of the ISO AMP module using a 12 V voltage regulator (7812) and a resistor voltage divider. A 5 V voltage regulator (7805), which would have been more appropriate for the task, was unavailable when we needed to construct this circuit.

laser beam. We installed shutters (Hi-Tec HS-5645MG) on the laser optical table in front of the fiber coupler of every fiber guiding light to the vacuum chamber table.

Shutter is an electrical device which can push or rotate an object at specific angles or distances. It consists of a motor, potentiometer, gear assembly and a controlling circuit. With the help of the gear assembly, a suitable position for the shutter blade is reached such that there is no electrical signal generated at the output port of the potentiometer. After that, an input signal is provided and compared with the output signal, which in turn is processed to generate a feedback signal. This feedback signal acts as an input to operate the motor. As the motor starts rotating the potentiometer knob also moves thus changing the output signal, when the output and the input signal become equal then the motor stops rotating. Figure 3.8 shows the various components of a shutter.

The angular position of the shutter can be manipulated by changing the width of Pulse Width Modulation (PWM) pulses , as shown in figure 3.9. The internal PWM module (micro-controller) can be programmed according to the requirements. Figure A.4 shows an excerpt from the code for controlling the shutters.

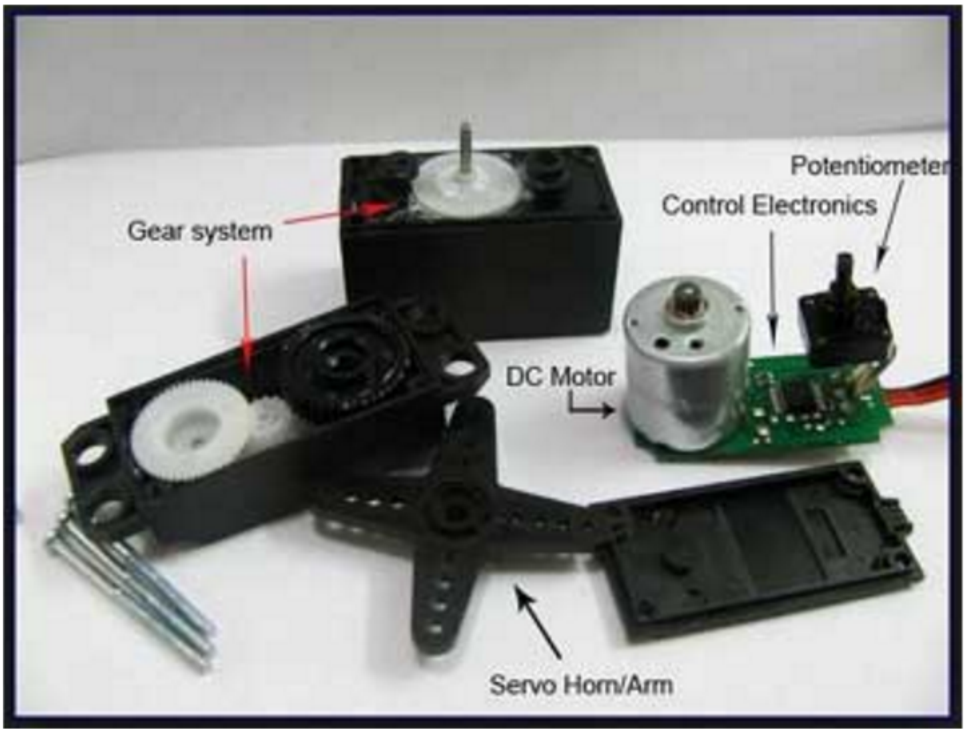


FIGURE 3.8: Shutter components [19].

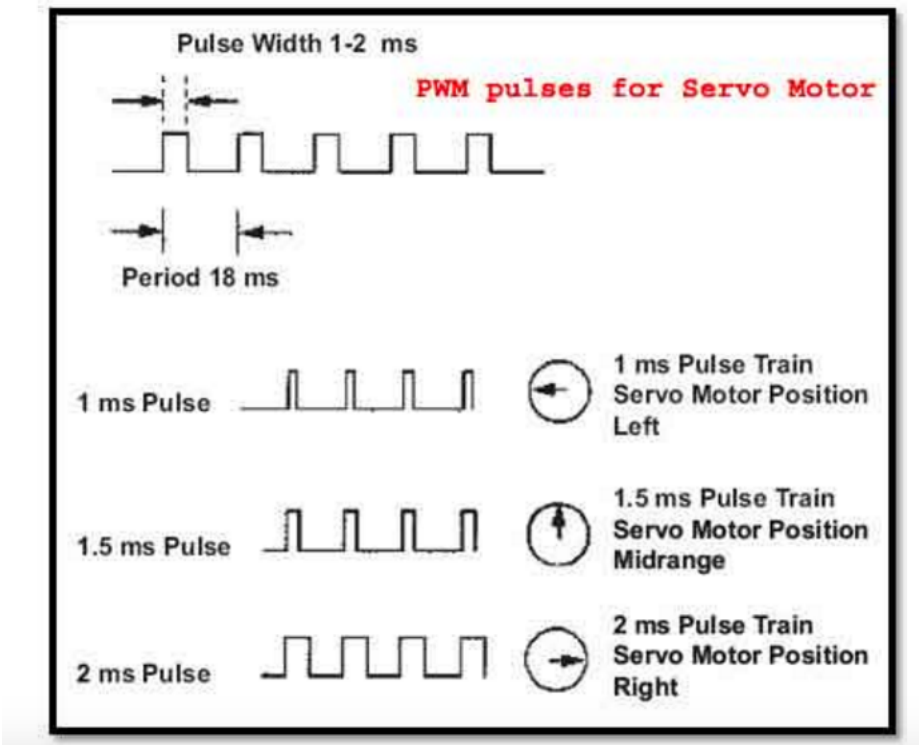


FIGURE 3.9: PWM of shutters [19].

Chapter 4

Master Laser

In order to trap and cool atoms in a MOT we require a well defined frequency coming out of the master laser. The frequency is decided in accordance with the particular atomic transition we want to address in our experiment. Hence, an external cavity diode laser was built [2], to suit the needs of the experiment.

4.1 Theory of External Cavity Diode Lasers (ECDL)

When a laser diode is placed in an external cavity it enables us to precisely tune the wavelength of the emitted light. This can be achieved by using the laser in the littrow configuration [10], which is depicted in figure 4.1. In this configuration an external cavity is formed between the rear facet of the laser diode and the diffraction grating. The rear facet of the laser diode usually has a high reflectivity when compared to the front facet (only few percent). An internal cavity is formed between the two facets but the feedback from the grating is much higher when compared to that from the front facet, thus the external cavity effect dominates. The external cavity determines the output wavelength.

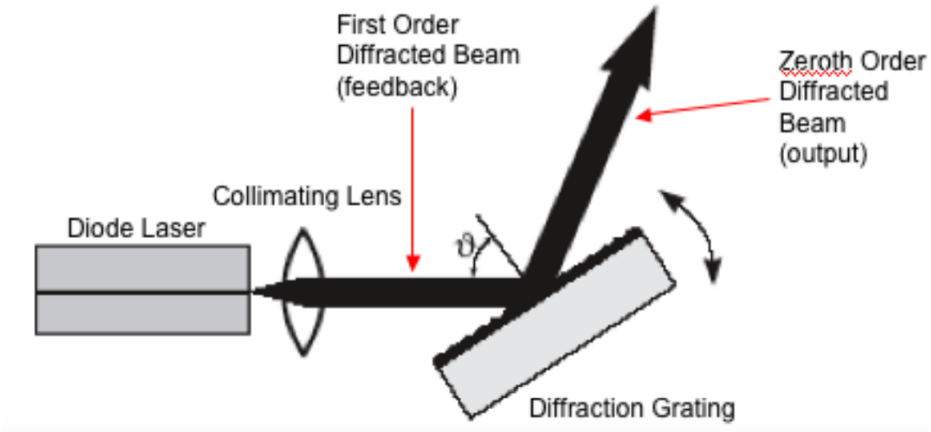


FIGURE 4.1: An ECDL in the Littrow configuration [10].

The wavelength of the master laser can be changed due to different effects. First, the angle of the diffraction grating can be moved with the help of a piezo, thus changing the wavelength of the minus first order diffraction, which is reflected back into the laser diode. Second, the length of the external cavity allows only certain frequency modes to exist within it. Tiny fluctuations in temperature causes thermal expansion, which leads to change in cavity length. Hence, the cavity resonance frequency is changed. The cavity resonance frequency is also changed due to fluctuations in current. When the current is changed, it leads to change in charge carrier density, thus changing the

refractive index and wavelength, which changes the resonance frequency. Hence, cumulative fluctuations in temperature and current can lead to the laser, hopping between different frequency modes [2]. Third, the doping of the laser diode, which determines its gain. This is determined by the manufacturer to centre the gain profile at the desired wavelength. It can be used to shift the profile a few ten nanometre up or down. It is also affected by temperature and current.

As the current is cranked up, at a particular value known as the threshold current the laser starts lasing i.e. there is an avalanche of stimulated emission and the frequency of the emitted light is well-defined. Figure 4.2 shows the output power versus input current graph at 767 nm. The threshold current is observed to be 55 mA.

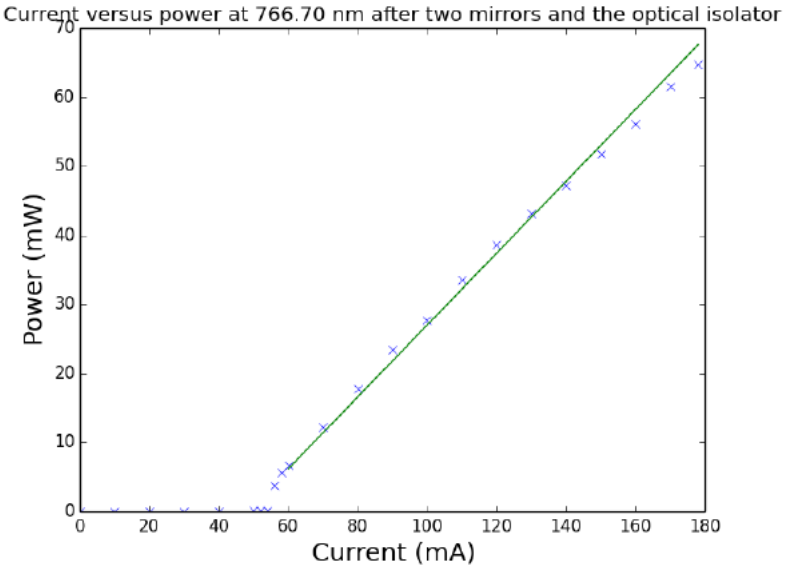


FIGURE 4.2: The output power vs input current of the laser at 767 nm. The threshold current is observed to be 55 mA [2].

4.2 Technical Specifications

The laser diode used is a SAL-780-100 diode from Sacher Lasertechnik and can be operated at a maximum current of 185 mA. The output of the laser diode is centered at 781.6 nm with FWHM of 10 nm, but it is operated at 767 nm, which leads to lesser output power. The temperature of the laser is monitored using a sensor (AD950) attached to the housing of the laser. The temperature is stabilised using a peltier, which is controlled by a PID using the temperature sensor as input. The piezo attached to the grating can be operated between 0 and 100 V.

Due to ageing of the diode the threshold current has increased significantly to 130 mA from 55 mA. This means that the diode will soon need to be replaced for long term use of the experiment. The laser output at maximum current is 25 mW and the operating temperature is 19.3°C, which is still risky since dewpoint in Amsterdam is quite high (can sometimes go upto 25°C!). In order to prevent condensation inside the laser, the laser's temperature should be above dew point of the laboratory environment. Hence being above 20°C is always advisable.

4.3 Aligning the Master Laser

The wavelength is tuned in two stages. First, rough tuning of the wavelength to a tenth of nanometer using a wavemeter by adjusting the screws. Then fine tuning it to thousandths of nanometer by changing the piezo voltage, which changes the grating angle, while using a potassium vapor absorption signal to tell if the correct wavelength has been reached (obtaining the absorption signal is the topic of the next chapter). Second, the laser output power needs to be maximised at the correct wavelength, which is done by aligning the reflection from the grating onto the light from the laser diode, until the maximum power is reached at the correct wavelength. Figure 4.3 shows a drawing of the master laser with its various components.

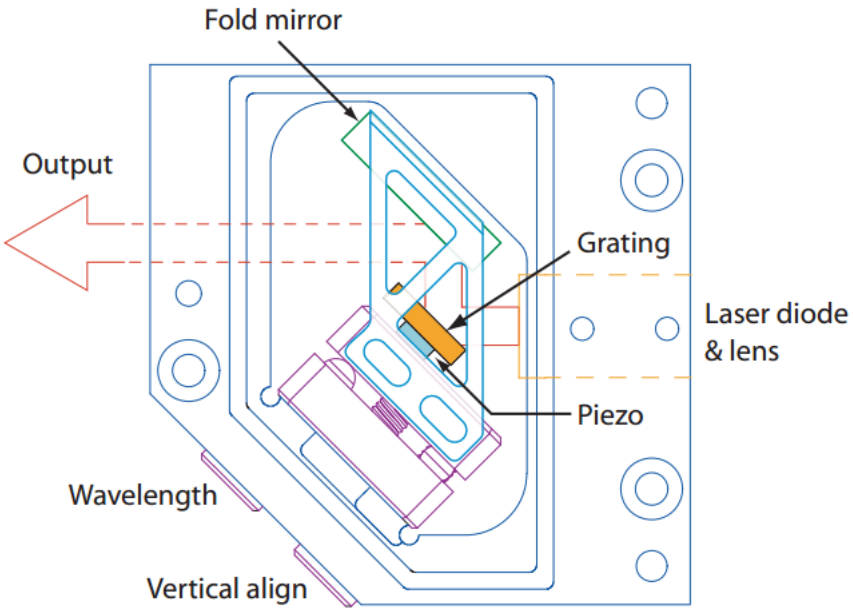


FIGURE 4.3: Schematic of master laser [20].

4.4 Experimental Insights

During this thesis the laser showed significant changes in its output. The grating got misaligned, leading to the emission of the wrong wavelength and a significant drop in the output power. The threshold current also increased significantly from 80 mA on 16.11.2015 to 150 mA on 26.06.2016. The laser output power also decreased significantly from 60 mW to 25 mW during the same time frame. The temperature of operation had to be lowered below dew point (17°C) to obtain 40 mW of power, which is a necessity for the experiment. This led to condensation inside the laser housing and on the grating (never clean the highly sensitive grating with anything!). The grating was replaced (with a similar type as before, 44% refelectivity), a half wave plate was installed to rotate the polarisation for enhancing the diffraction efficiency of the grating and the alignment for getting the correct wavelength and power had to be redone. A nitrogen flow inlet was also installed inside the laser housing to prevent condensation.

Chapter 5

Laser Lock Setup

Since the master laser can drift from the desired frequency and hop between different frequency modes due to fluctuations in temperature and current, a feedback loop is required for preventing this phenomenon. The purpose of the laser lock setup is to prevent the drift of the laser, from the desired wavelength of operation. The phenomenon used in the laser lock setup is called Doppler-free DAVLL spectroscopy [11].

5.1 Doppler-Free Spectroscopy

When a laser beam (photons) of a particular frequency is shone into a cloud of atoms, all the atoms will not observe the actual frequency (ν) of the photons, instead atoms with a velocity component along the laser beam will observe a shifted frequency known as the Doppler shifted frequency ($\nu^{'}$), given by

$$\nu' = \nu + \frac{2\pi v}{\lambda}, \tag{5.1}$$

where v is the velocity of the atom and λ is the wavelength of photon. This phenomenon is known as Doppler effect [11]. Hence, the cloud of potassium atoms can even absorb photons of several different frequencies depending on the velocity of the atoms in the clouds. Hence, one and the same transition needs a different laser frequency, depending on the velocity component of the atom along the laser beam, which leads to a Doppler broadened absorption signal, depicted in figure 5.1 [12].

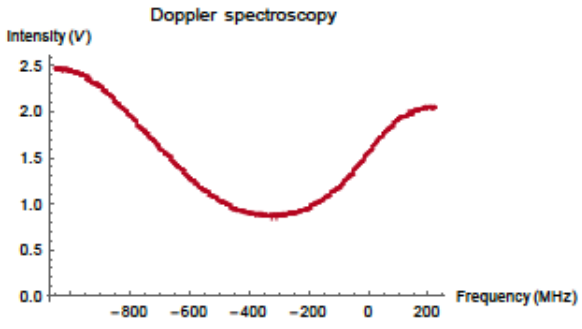


FIGURE 5.1: Doppler spectroscopy signal [12].

The width of Doppler spectrum is around 800 MHz, which doesn't allow stabilization of the laser frequency to the desired amount. Because the line of interest is only 6 MHz wide, and a MOT needs a stability on that order. To overcome this difficulty we shine light from two counter-propagating directions (pump and probe beam) of the

desired frequency, instead of one. The pump beam usually has ten times higher intensity and the probe beam has the same intensity as that of saturation intensity. As both beams are resonant with atoms of a different velocity class, as depicted in figure 5.2(b), they will get absorbed and drive atomic transitions in atoms with opposite direction but equal magnitude of the velocity component along the probe beam (figure 5(a)). When both beams address the atoms with no velocity component along the propagation direction of the beam of atoms as depicted in figure 5.2(d), then the pump beam saturates the transition of atoms of this velocity class, and the probe beam can pass through the vapor without being absorbed (figure 5(c)). This happens exactly if the laser beams have the desired frequency, since the addressed velocity class of the atoms are stationary along the propagation direction of the beams and do not experience a Doppler shift [11].

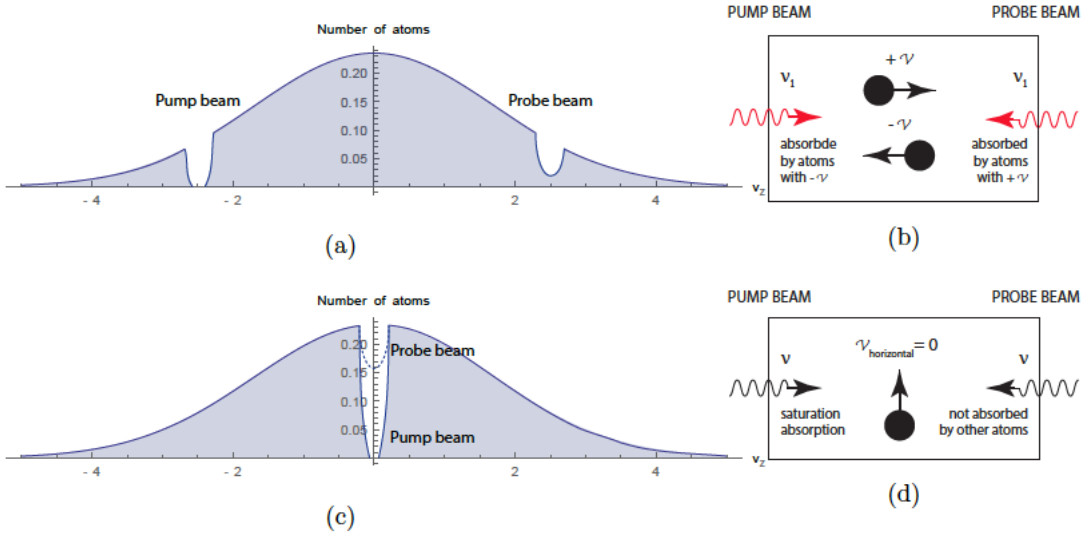


FIGURE 5.2: Principle of Doppler-free spectroscopy [12].

5.2 DAVLL Spectroscopy

Figure 5.3 shows the Doppler-free saturation absorption signal, which is a symmetric spectroscopy signal (figure 5.4(a)) of the desired frequency but it is not suitable for locking the laser. For that an anti-symmetric signal (figure 5.4(b)) is required, which gives information about whether the laser is drifting towards higher or lower frequencies and correspondingly adapting a mechanism to bring it back to the desired frequency. We obtain the desired spectroscopy signal using DAVLL spectroscopy, which we have implemented in our laser lock setup.

To implement this technique magnetic field is required, which can split the energy levels of the magnetic states, as depicted in figure 5.5. This phenomenon is known as the Zeeman effect. Next, the polarisation of the laser beams needs to be understood. The pump and probe beams are both linearly polarized. They need to be considered as an equal superposition of right-handed circularly polarized (RHCP) light and left-handed circularly polarized (LHCP) light. The magnetic field is applied parallel to the direction of the pump beam, hence $\sigma^+$and σ^- transitions are driven by RHCP and LHCP respectively. At one specific frequency, only one type of transition occurs [3], hence leaving the remainder of the probe light elliptically polarized. This light can be split into orthogonal polarisations using a quarter wave-plate (QWP) and a polarizing

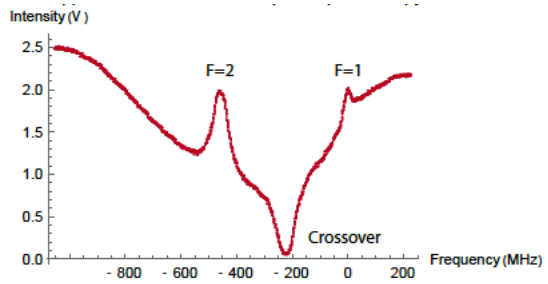


FIGURE 5.3: Doppler-free saturation absorption signal [12].

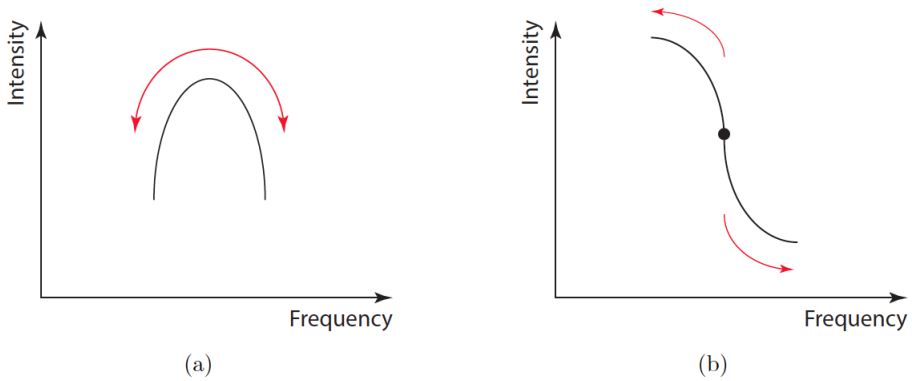


FIGURE 5.4: Symmetric signal (a), Anti-symmetric signal (b) [12].

beam splitting cube (PBC), which are sent onto two photo-diodes followed by their subtraction to give a dispersive signal, as depicted in figure 5.6.

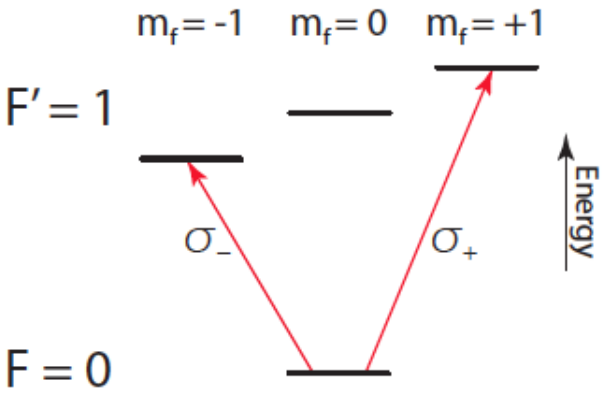


FIGURE 5.5: Zeeman splitting in magnetic states [12].

5.3 Optical Setup and Electronics

Figure 5.7 illustrates the optical setup of the laser lock. The frequency of the laser is red shifted from the laser lock atomic transition ($^2S_{1/2}$, $F'=1 \rightarrow {}^2P_{3/2}$ of figure 2.2) by an amount equal to the frequency of the spectroscopy AOM (Spectro in figure 5.7). We

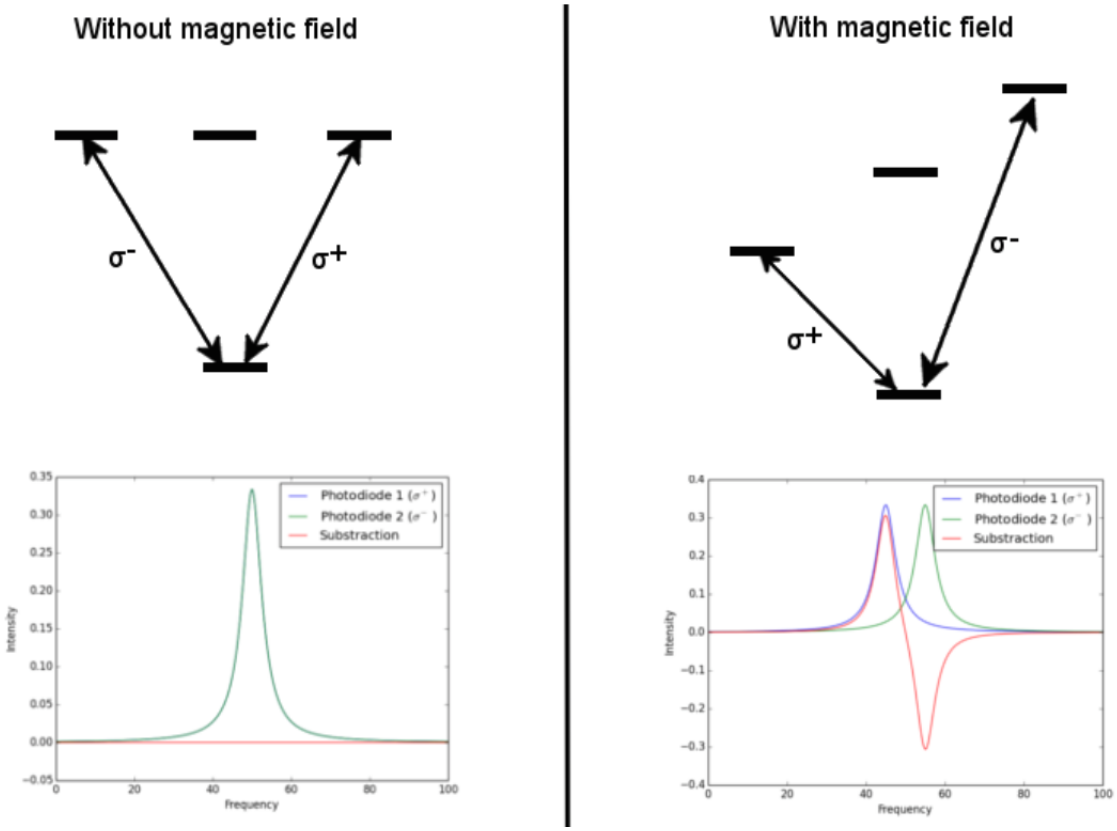


FIGURE 5.6: Principle of DAVLL spectroscopy [2].

use the most abundant isotope of potassium (^{39}K), hence making it easier to find the spectroscopy signal.

Feedback electronics is required for correcting the slow and fast changing drifts of frequency from the desired value. This is achieved by constructing a proportional-integrator-differentiator controller (PID). The proportional part measures the difference between the incoming signal and a reference signal (here: zero voltage) and proportionately provides a correction. The integrator sums over this difference over a certain time and then provides a correction proportional to that integral, which helps to null the error signal over long times. The differentiator measures the change in difference over a certain time and provides a correction proportional to that change, which suppresses oscillations of the PID loop.

5.4 Measurements and Results

5.4.1 Laser Characteristics

Laser Diode Current	-182 mA
Piezo Voltage	48.8 V
Temperature	19.3°C
Laser Output Power	25 mW

TABLE 5.1: Laser Mode characteristics at lock point.

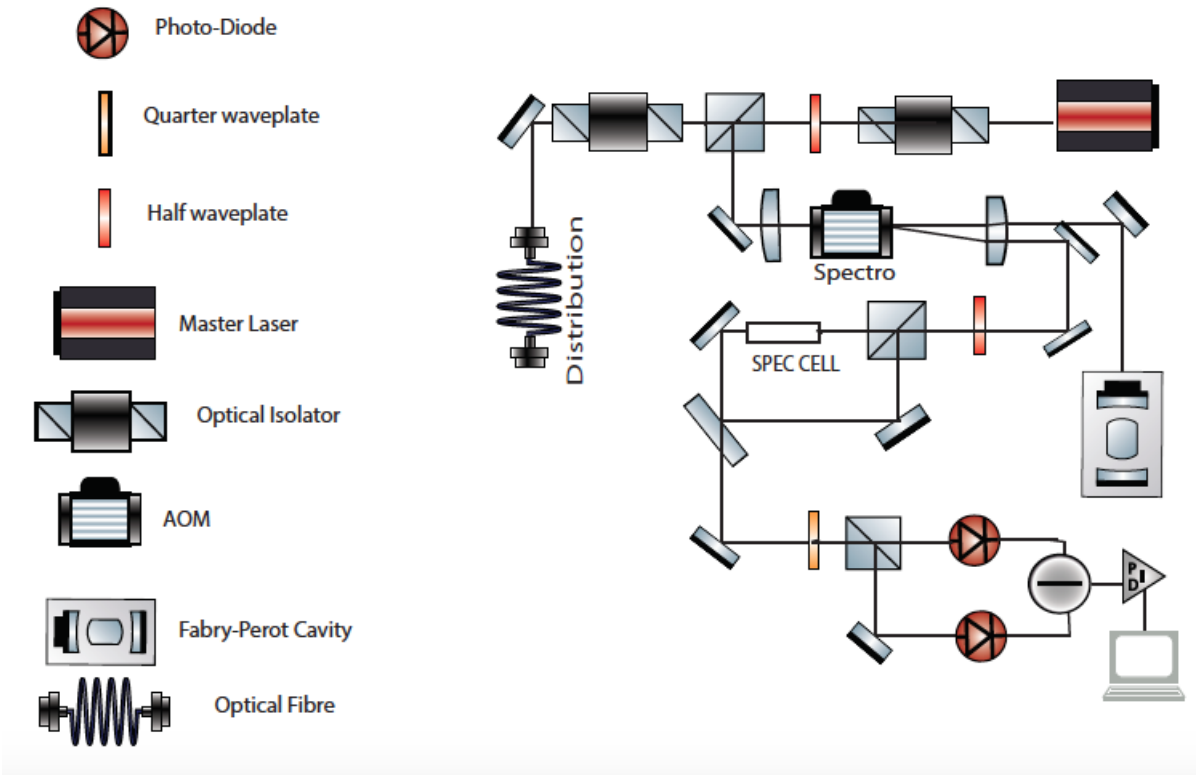


FIGURE 5.7: Laser lock setup.

Table 5.1 shows the measured values of the laser mode characteristics at lock point. It is always necessary to lock on this same mode of the laser since the output of the laser is fibre coupled to the rest of the experiment, otherwise the fibre will not remain injected. This happens because the grating reflects the laser beam into different directions for different modes.

5.4.2 Spectroscopy AOM Characteristics

The AOM used is (Gooch and Housego 3200-124). The central frequency of the AOM has been tweaked manually by changing the oscillator [2]. The new value was measured using a signal generator, directional coupler and oscilloscope, and is 283±2 MHz with a bandwidth (FWHM) of 5 MHz. Table 5.2 gives the measured characteristics of the AOM.

Frequency	-282.3 MHz
RF Attenuation	8 dB
Diffraction Efficiency	52.4%

TABLE 5.2: Spectroscopy AOM characteristics.

5.4.3 Spectroscopy Cell Characteristics

Table 5.3 states the measured characteristics of the spectroscopy cell.
The magnetic field (B) created in the spectroscopy cell can be calculated using

Temperature	68°C
No of turns per unit length (n)	10 turns/cm
Current (I)	0.8 A

TABLE 5.3: Spectroscopy Cell Characteristics

$$B = \mu_{\circ} n I, \tag{5.2}$$

where $\mu_{\circ}$is the permeability in free space. After calculation, B is $10.048G$.

5.4.4 Laser Lock Characteristics

Figure 5.8 shows the absorption and dispersive spectroscopy signal for the F$'$=1 and F$'$=2 transition of $^2S_{1/2}$ state (figure 2.2). We are interested in locking on the F$'$=1 transition. A good dispersive signal is considered to be 100 mV peak to peak which matches excellently with the measured value. The laser lock was observed to be stable for atleast a day.

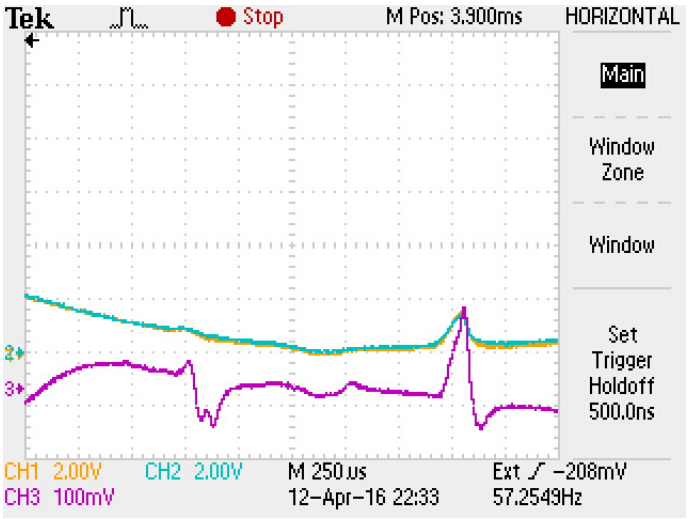


FIGURE 5.8: The purple curve is the dispersive signal, (left) F$'$=1 and (right) F$'$=2 transition of $^2S_{1/2}$ state. The yellow and blue curves are absorption signals for these transitions corresponding to two different polarizations (σ^+ and σ^-).

5.4.5 Knife-Edge Measurement

A knife edge measurement was performed to calculate the waist of the laser output beam after the spectroscopy AOM. This measurement was required to calculate the intensities of the pump and probe beams used for the laser lock spectroscopy. The measured values of beam power versus position of the knife-edge (figure 5.9) were fitted to the function (Origin software) given by

$$P = \frac{A}{2} \times erfc[\sqrt{2}(\frac{x - x_{\circ}}{w})], \tag{5.3}$$

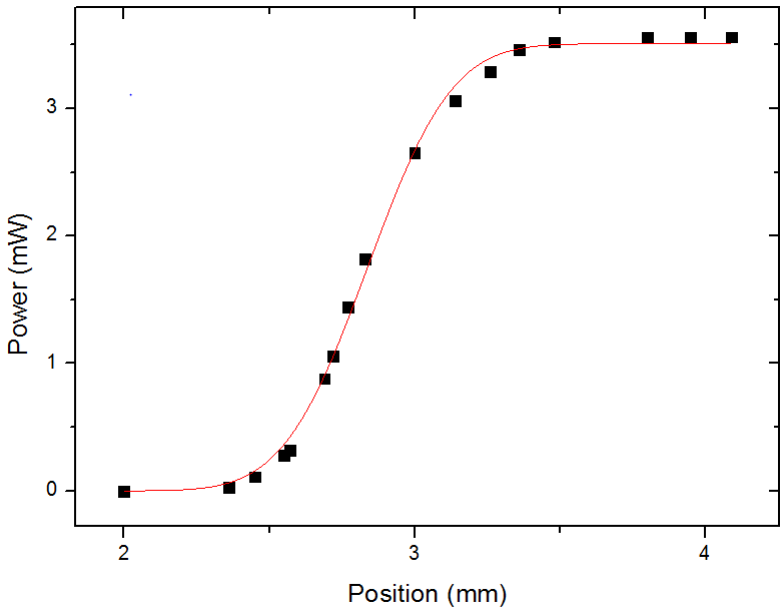


FIGURE 5.9: Knife-edge measurement.

where w is the beam waist, A is $P_{\max}$, $x_\circ$ is the position at which $P_{\max}/2$ is attained. The values of the above stated parameters has been calculated using Origin software. This is stated in table 5.4,

Parameter	Value	Standard Error
A (mW)	3.51	0.03
$x_\circ(mm)$	2.838	0.007
w (mm)	0.46	0.02

TABLE 5.4: Knife-edge fit parameters.

5.4.6 Beam Intensity Calculations

Table 5.5 gives the measured pump and probe powers.

Pump Power (P_{pump})	0.67 mW
Probe Power (P_{probe})	0.055 mW

TABLE 5.5: Pump and probe powers.

The Intensity (I) of the beam can be calculated using

$$I = \frac{2P}{\pi w^2}. \tag{5.4}$$

The calculated intensities of pump and probe beam is given by Table 5.6.
Hence the pump beam is able to saturate the atoms, thus making the probe beam transparent to the atoms.

Pump Intensity (I_{pump})	201.68 mW/cm^2	115 I_{sat}
Probe Intensity (I_{probe})	16.6 mW/cm^2	10 I_{sat}

TABLE 5.6: Pump and probe intensities.

5.4.7 Simulations

Simulations of the absorption signal were performed in order to better understand the excited state hyperfine splitting of the ^{39}K transition to which we lock (figure 2.2). Since the hyperfine splitting cannot be resolved due to its narrow structure, it cannot be precisely determined to which hyperfine state the laser is locked. Selection rules allow only $\delta m = 0, \pm 1$ transitions [3].

First, the Zeeman frequency shifts (F_{Zeeman}) of the individual magnetic states (m) of the various hyperfine states, in the presence of an external magnetic field (B) needs to be calculated using [3]

$$F_{\text{Zeeman}} = \frac{g_{\text{F}} \mu_{\text{B}} m B}{h}, \tag{5.5}$$

where m ranges from -F to F, g_{F} can be calculated for different hyperfine states using

$$g_{\text{F}} = \left(1 + \frac{\text{J(J+1)} + \text{S(S+1)} - \text{L(L+1)}}{2\text{J(J+1)}}\right) \times \left(\frac{\text{F(F+1)} + \text{J(J+1)} - \text{I(I+1)}}{2\text{F(F+1)}}\right), \tag{5.6}$$

where J=L+S and I=3/2 for ^{39}K [3]. Second, the dipole transition matrix (DM) for the various σ^+ and σ^- transitions from ground (1) to excited (2) state can be calculated using

$$\begin{aligned}\text{DM} = \sqrt{(2\text{J}_1+1)(2\text{J}_2+1)(2\text{F}_1+1)(2\text{F}_2+1)} \times \begin{bmatrix} L_2 & J_2 & S_1 \\ J_1 & L_1 & 1 \end{bmatrix} \\ \times \begin{bmatrix} J_2 & F_2 & I \\ F_1 & J_1 & 1 \end{bmatrix} \times \begin{pmatrix} F_1 & 1 & F_2 \\ m_1 & \delta m & -m_2 \end{pmatrix},\end{aligned} \tag{5.7}$$

where $\delta m = m_2 - m_1$ and the first two matrices are Wigner-6j symbols and the last one is a Wigner-3j symbol [3]. DM for the various transitions have been calculated using Mathematica. Third step, is to calculate the on resonance saturation parameter ($s_\circ$), given by

$$s_\circ = \frac{I_{\text{probe}}}{I_{\text{sat}}}. \tag{5.8}$$

The final step is to calculate the scattering rate (Γ_{sc}) [4] from all the transitions and sum them up to get the total contribution, Γ_{sc} is given by

$$\Gamma_{\text{sc}} = \frac{\Gamma}{2} \times \left(\frac{\text{s}_\circ \text{DM}}{1 + \text{s}_\circ \text{DM}}\right) \times \left(\frac{1}{1 + (\frac{2\delta}{\Gamma'})^2}\right), \tag{5.9}$$

where $\delta = x - F_{\text{Zeeman}} + F_{\text{AOMSpectro}}$ (x is the scanning laser frequency); and $\Gamma' = \Gamma\sqrt{1 + \text{s}_\circ}$ is the power broadened line-width. After calculations, Γ_{sc} vs x has been plotted for different values of B and $s_\circ$. In the following graphs (5.10, 5.11, 5.12, 5.13), the zero of the frequency axis is the atomic transition to which we lock. The FWHM

is estimated to be $2\Gamma'$. Figure 5.14 shows the comparison between experimental and theoretical dispersive signal.

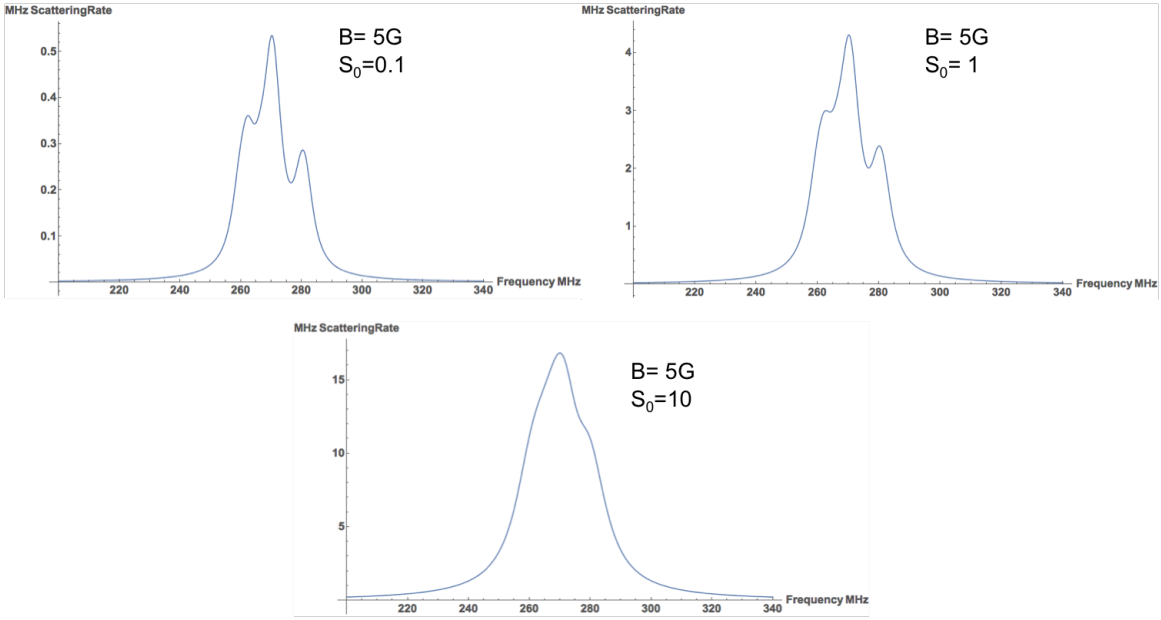


FIGURE 5.10: Calculated laser lock absorption signal.

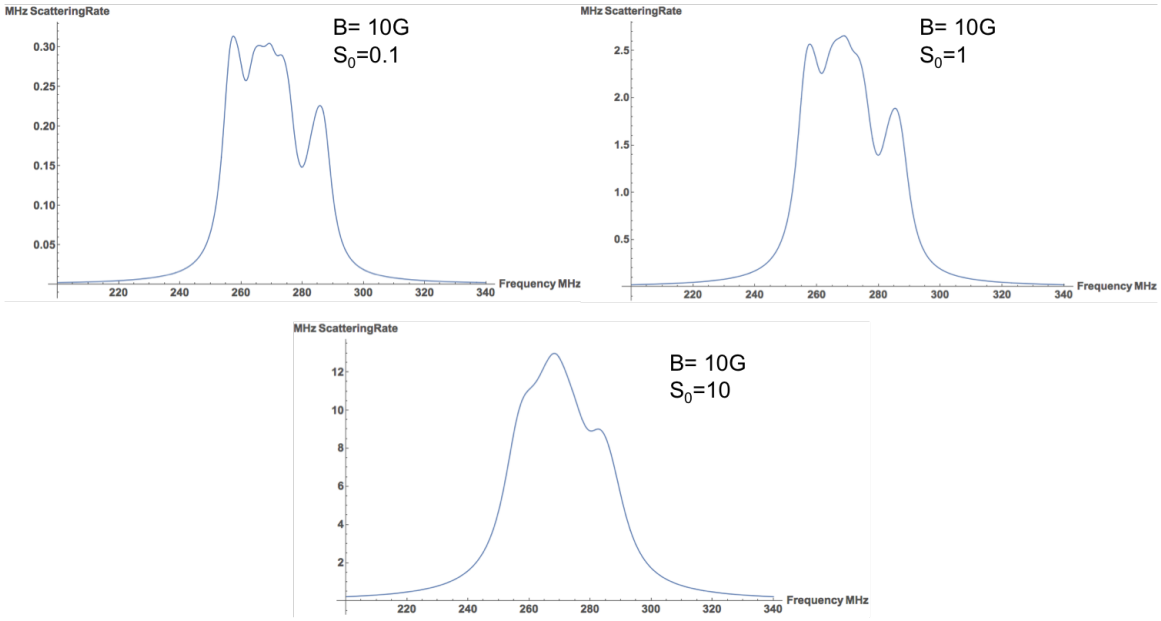


FIGURE 5.11: Calculated laser lock absorption signal.

The experimental regime corresponds to B=10 G and $s_\circ = 10$. Power broadening ($s_\circ = 10$) is observed in both theoretical and experimental results (figure 5.8). Hence, the distinct transitions due to Zeeman splittings gets aliased instead of being well separated. In the non-power broadened regime ($s_\circ = 0.1$) individual distinct transitions are visible, when Zeeman splittings are greater than the line-width of the atomic transition. At B=50 G a clear distinction can be made between the σ^+ transitions (right) and σ^- (left). In order to manifest the multiple level optical Bloch solutions into a two-level solution, the contributions from various two-level transitions are summed. In potassium Zeeman splitting is 1.4 MHz/G [3,4].

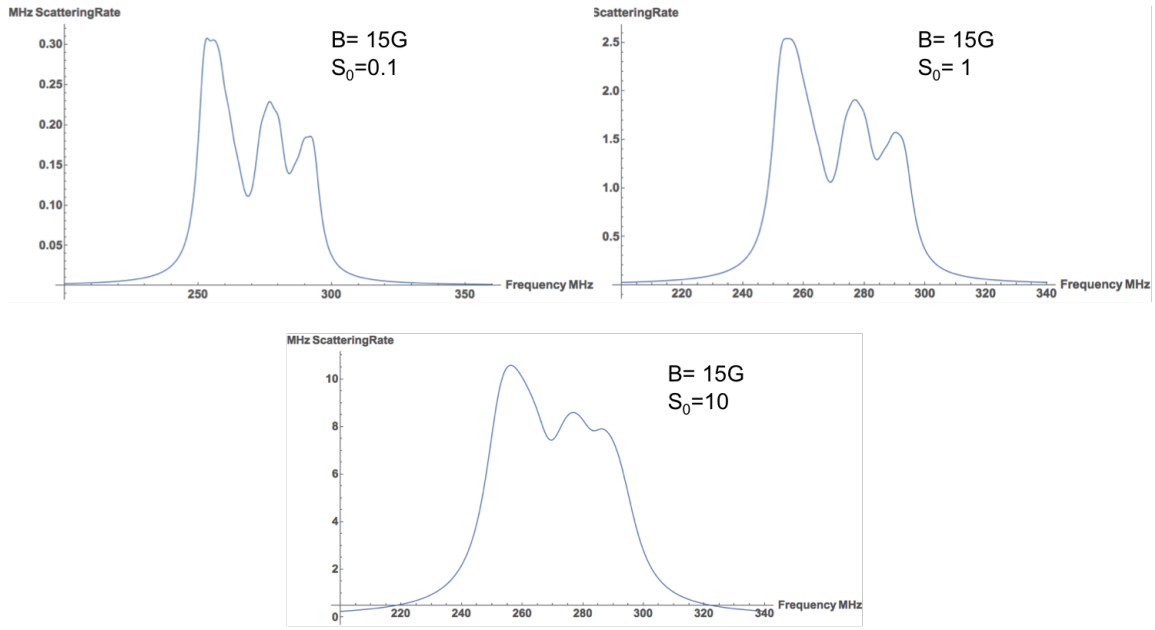


FIGURE 5.12: Calculated laser lock absorption signal.

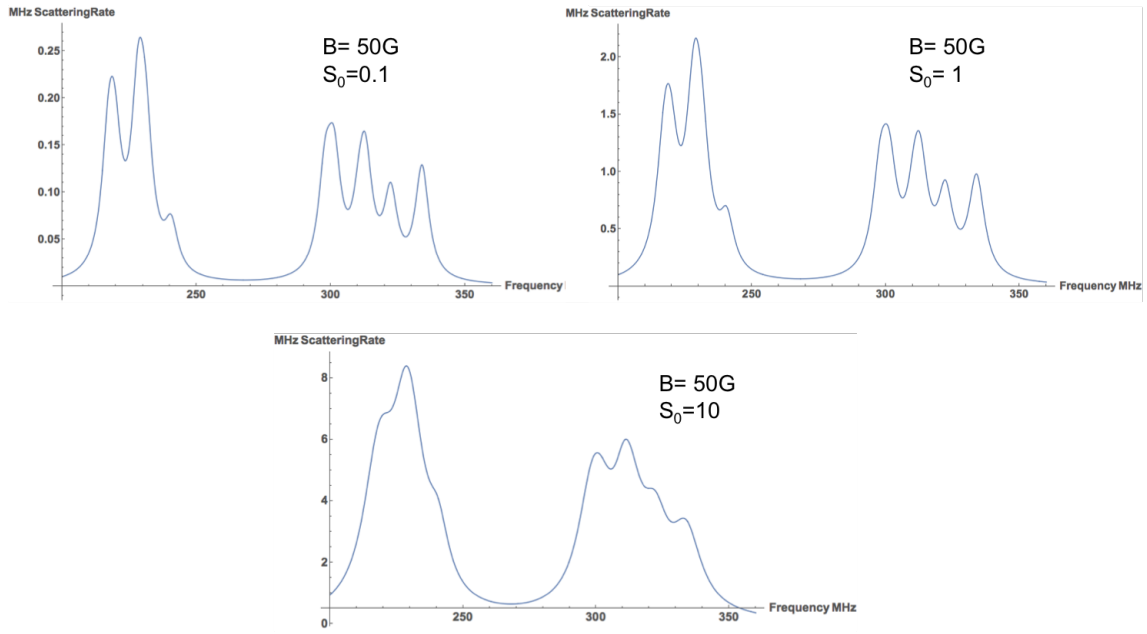


FIGURE 5.13: Calculated laser lock absorption signal.

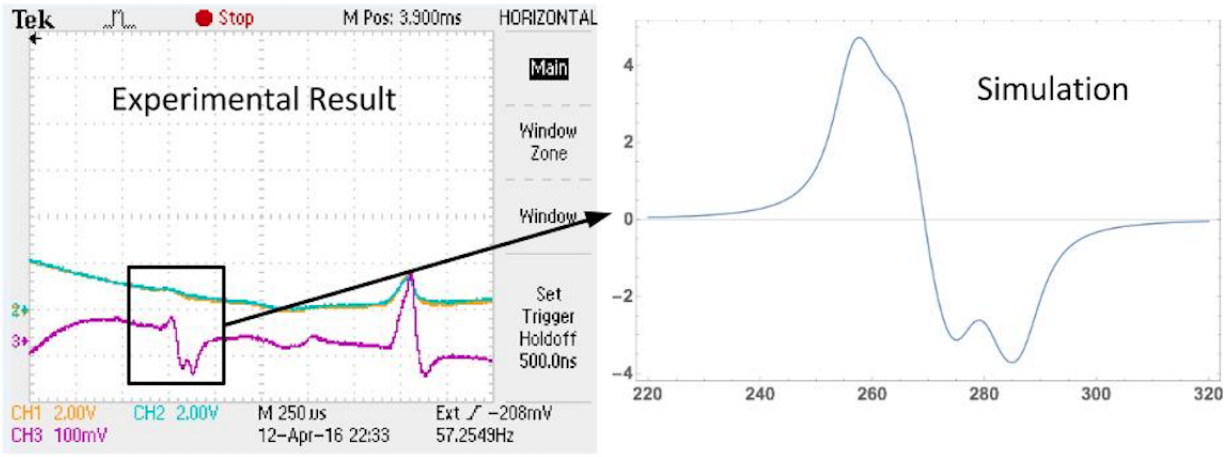


FIGURE 5.14: Experimental and theoretical dispersive signal used for locking the laser.

Chapter 6

Amplifier Setup

The various components used in the amplifier setup will be explained and illustrated in this chapter.

6.1 Tapered Amplifiers

We use three tapered amplifiers (TAs) in our experiment for amplifying the laser light. The TAs use a semiconductor chip, which is (Eagleyard EYP-TPA-0765-01500-3006-CMT03-0000). The TAs have a special tapered geometry, which is broad at the output facet and narrow at the input facet. The TAs are seeded with light from the master laser, which gets amplified by stimulated emission inside the chip, due to a large gain medium. The input facet is a waveguide designed to enable operation on a single spatial mode. At high light intensities the semiconductor output facet is damaged. In order to avoid that a TA has a wide output facet, for reducing the intensity of the light exiting from the semiconductor. Figure 6.1 illustrates a tapered amplifier [13].

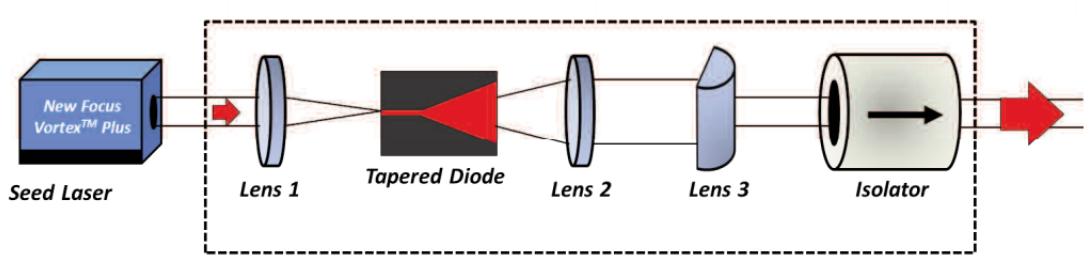


FIGURE 6.1: Tapered amplifier [13].

The TAs used in the experiment are mounted on a home-made housing which did not turn out to be very stable, as the pointing of the laser beam changed considerably over a day. The solution was to glue the peltier with vacuum glue to the housing, and as of when this thesis was being written the pointing of the TA output beam did not seem to move considerably. The TAs had to be re-injected throughout the thesis, since the stability issue was not solved until the end. The TAs are temperature controlled using Thorlabs temperature controllers. The temperature needs to be above dew-point for preventing condensation on humid days. Simultaneously the output power should also be optimum for the experiment. All the TAs have a constant nitrogen flow to prevent condensation on the chip. One of the TAs requires additional water cooling for temperature stabilisation. All the TAs were temperature stabilised using a PID, after questing the maximum power out of them, by optimising the position of collimation lens.

Since the chip has a rectangular geometry, cylindrical lenses have been used to deform the rectangular mode to a square mode, but still the mode is not perfectly Gaussian hence the coupling efficiency into the fibres is limited to only fifty percent. Also, it is very crucial to ensure that no light gets back reflected into the TAs, thus leading to damage of the chip. To ensure this, optical isolators have been installed after each of the TAs. It was also noticed that the flourescence from the TAs was reaching up to the master laser, hence two optical isolators were installed after the master laser.

6.2 Acousto-Optic Modulators

AOMs are devices which helps us in precisely tuning the frequency of laser light for suiting our experimental needs. An AOM comprises a piezo element attached to a piece of glass or a crystal. When the piezo element is supplied with a RF signal, it creates an acoustic wave inside the crystal, having the same frequency as that of the RF signal. This acoustic wave are periodic planes of compressions and rarefactions, which lead to change in refractive index, thus forming a diffraction grating inside the crystal. When light is incident on the grating, if it satisfies Bragg condition, then it can be diffracted into the first order (the one usually of interest). The frequency shift (ΔF) of the laser beam after the AOM, in the first order ($m = +1$) is the same as the frequency of the acoustic wave (F). This is due to Doppler effect (equation 6.1), as light is getting scattered from moving planes. The intensity of the beam can be modulated by changing the RF intensity, which in turn changes the amplitude of the acoustic wave. Figure 6.2 presents an illustration of an AOM.

$$\Delta F = m \times F \tag{6.1}$$

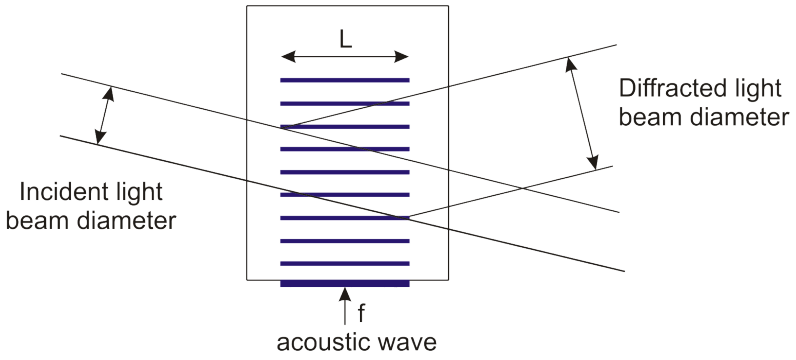


FIGURE 6.2: Acousto-optic modulator [21].

All the AOMs after the TAs, except two, are ISOMET-1205 AOMs with central frequency at 80 MHz and bandwidth of 30 MHz. The trap to repump AOM (figure 6.5) is custom made (Brimrose GPF-1240-200-766), which is used to shift the frequency by 1.2435 GHz. These AOMs are in single pass configuration, where a telescope system of lenses is used to focus light into the AOM and later having a collimated output beam. All AOMs had to be realigned and some of the optomechanics had to replaced and rebuild. The imaging AOM was newly installed. It is a double-pass AOM, where a telescope is followed by a quarter wave plate and a retro-reflecting mirror hence diffracting the beam twice. The AOM is from Isle Optics, LMO55-F (with a non-existing datasheet, it is one of the antiques!). The central frequency was measured to be 58 MHz and bandwidth as 20 MHz. The imaging AOM crystal was burnt near one of the edges, hence the transmission was significantly reduced, but it was adapted by making the entry hole

for the beam bigger, so that the whole crystal is visible and the beam hits on the other edge.

6.3 Optical Fibres

An optical fibre is a dielectric waveguide which transmits light along its axis by the process of total internal reflection. It consists of two layers, core and cladding (figure 6.3). For total internal reflection to happen, light should be incident at the core-cladding interface at an angle greater than the critical angle (i_{critical}), given by equation 6.2. Hence refractive index (n) of the core must be higher than that of the cladding. Given this information, for light to be guided inside the fibre, the range of acceptable entry angles (Θ) of light can be calculated, given by equation 6.3.

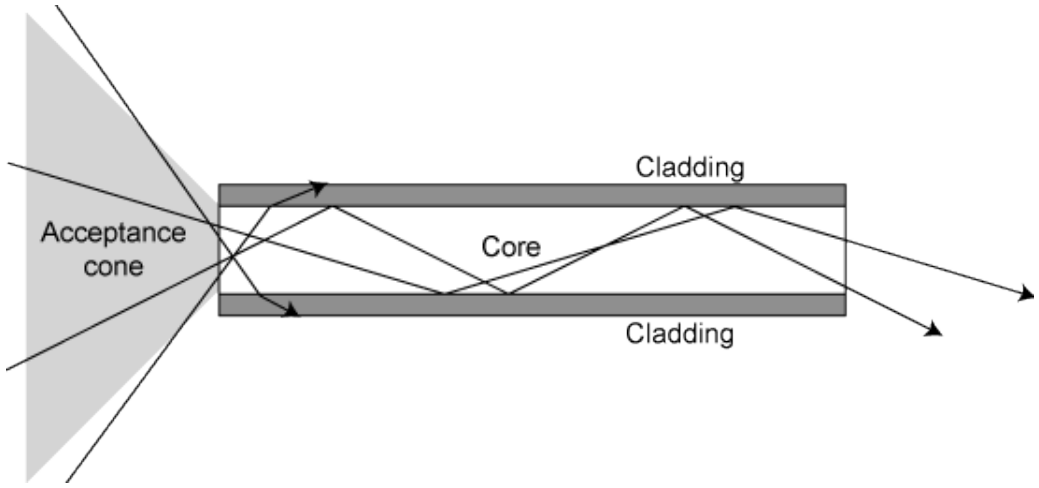


FIGURE 6.3: Optical fibre [22].

$$i_{\text{critical}} = \sin^{-1}\left(\frac{n_{\text{cladding}}}{n_{\text{core}}}\right) \tag{6.2}$$

$$\Theta \leq \sin^{-1}\left(\sqrt{n_{\text{core}}^2 - n_{\text{cladding}}^2}\right) \tag{6.3}$$

A special category of fibres are polarisation-maintaing fibres. They have a systematic linear birefringence [1] in the fibre so that the vertical and horizontal polarization modes traverse with distinct phase velocities inside the fibre. The fibres used in the experiment, work on the principle of stress birefringence, which is implemented by using a rod of a different material than the cladding and putting it within the cladding. Figure 6.4 illustrates a polarization maintaing fibre (Panda Style).

Optical fibres are an integral part of the experiment for both transporting light and isolating different sections of the experiment. Optical fibres from Thorlabs and Schäfter + Kirchhoff are used. They have a cutoff wavelength slightly lower than 767 nm, which is the wavelength of interest. All the fibres are single mode, polarization maintaining, except the one going to the wavemeter, which is a multi-mode fibre. The diameter (ϕ) of the beam coming out of the fibre is given by

$$\phi = 2 \times 0.82 \times NA \times f, \tag{6.4}$$

[1] Property of a material where the refractive index is dependent on polarization and propagation direction of light.

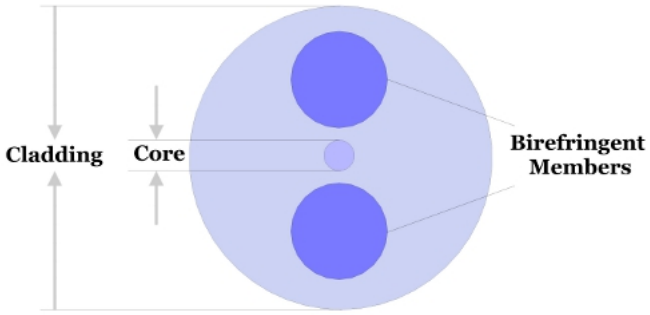


FIGURE 6.4: Polarization maintaining fibre [23].

where NA is the numerical aperture of the fibre and f is the focal length of the fibre collimator lens. This information can sometime save some time and effort to do a knife-edge measurement.

The main distribution fibre from the laser isolates the whole experiment from any misalignment in the laser. The 2D MOT, 3D MOT, push and imaging beams are transported to the vacuum table using optical fibres (figure 6.5). All the fibres have been re-injected, and some of the optomechanics had to be rebuilt. The imaging fibre and optomechanics was newly installed. The polarisation of all the fibres have been maintained, by rotating the fibre collimator or a half-waveplate (in front of the fibre), and aligning it with the axis of polarisation of the incoming linearly polarized light using a polarimeter. To provide better stability for the experiment, fluctuations in power after the fibre should be minimised as much as possible by injecting the fibers such that the polarization is maintained. These fluctuations will only be noticeable if there is a polarization sensitive component after the fibre.

6.4 Experimental Insights

Now that we have a overview of the optical components used for building the optical setup as well as know their importance, one can start talking about the necessity to put together all these components and build a powerful setup (figure 6.5), which can be used to study interesting physical phenomena.

For cooling and trapping atoms, the power from the master laser is insufficient. Hence TAs are required to increase the power. The master laser only provides 25 mW, way lesser than previously [2]. Earlier [2], the power from the master laser was sufficient to seed the two TAs, K Trap and K Mix but now it is insufficient. Hence the setup had to be modified to suit the needs of the experiment. Currently, the master laser power is sufficient to seed only one TA. Hence K Mix is seeded by the master laser, and some light is taken after the K Mix to seed the K Trap, as illustrated in figure 6.5.

Figure 6.6 shows the various frequencies which are required for the experiment. The trap and the repump beam are both slightly red detuned from their respective transitions. The repump light is required for cycling the atoms back to the trap transition, otherwise a significant amount of atoms will be lost. The repump light is shifted by 1.2435 GHz from the trap light, using a Brimrose AOM, the output of this AOM is injected into a fibre which seeds the K repump TA, and after that we have enough power for the repump transition. There are two sets of trap and repump light for the 2D and 3D MOTs. The trap and the repump light is later made to recombine, separately for

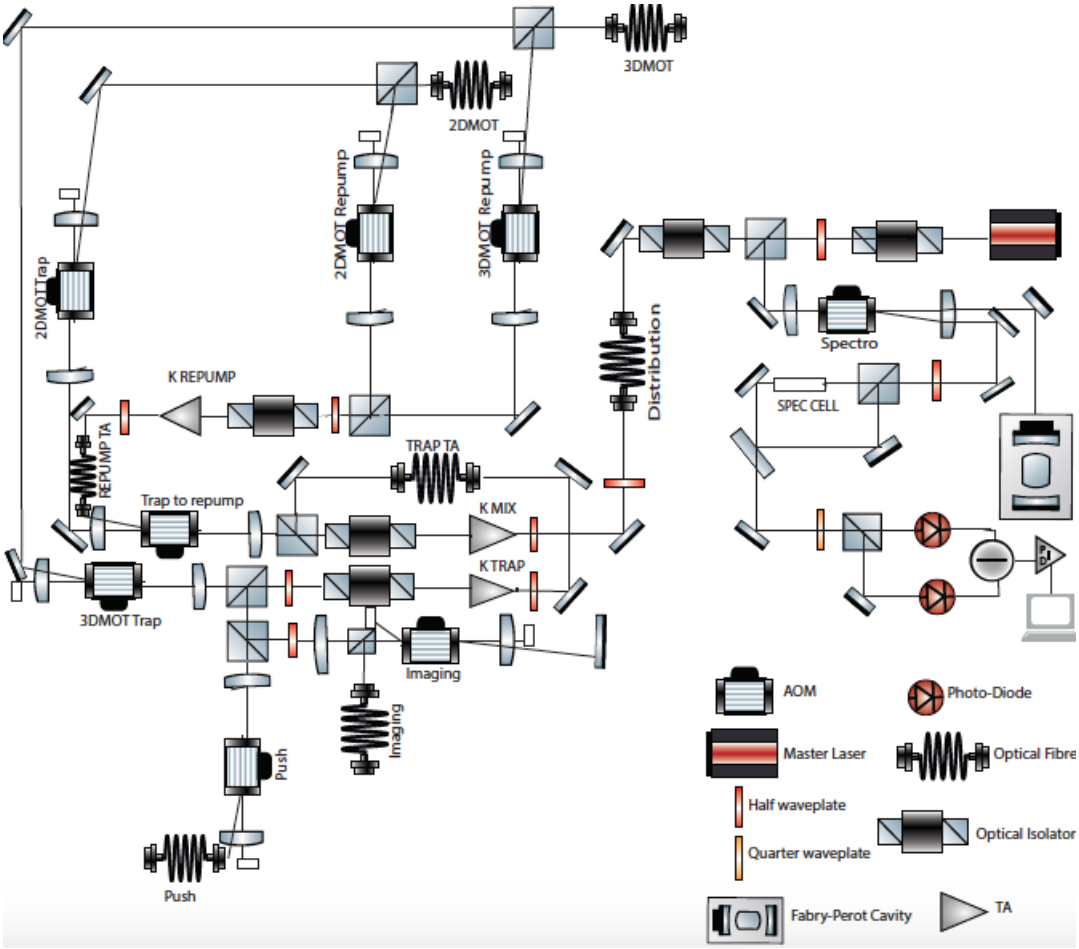


FIGURE 6.5: Amplifier and laser lock setup.

both the MOTs, using a PBC. To have a good coupling efficiency for both the beams, the beam waist and collimation should be the same. A push beam is used for transferring the atoms from the 2D MOT to the 3D MOT chamber.

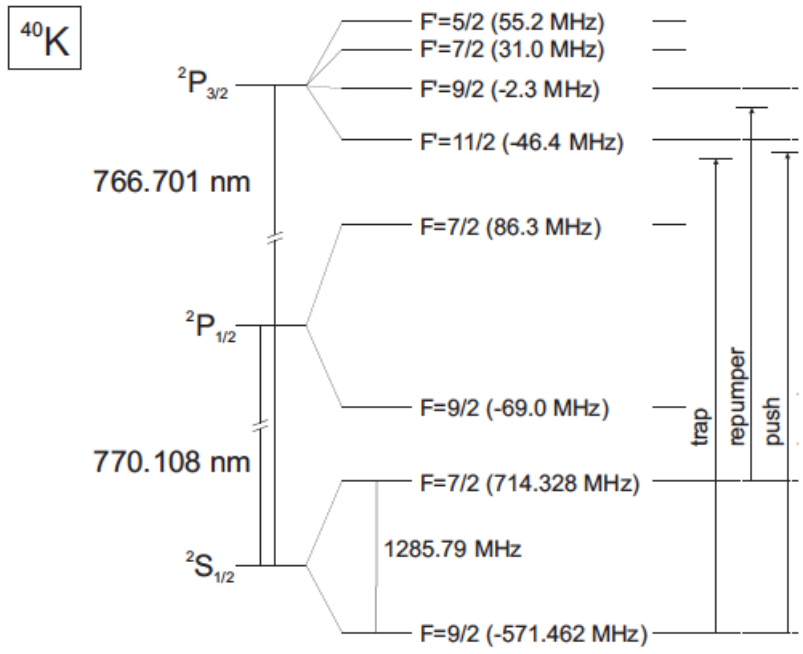


FIGURE 6.6: Level scheme of ^{40}K [2].

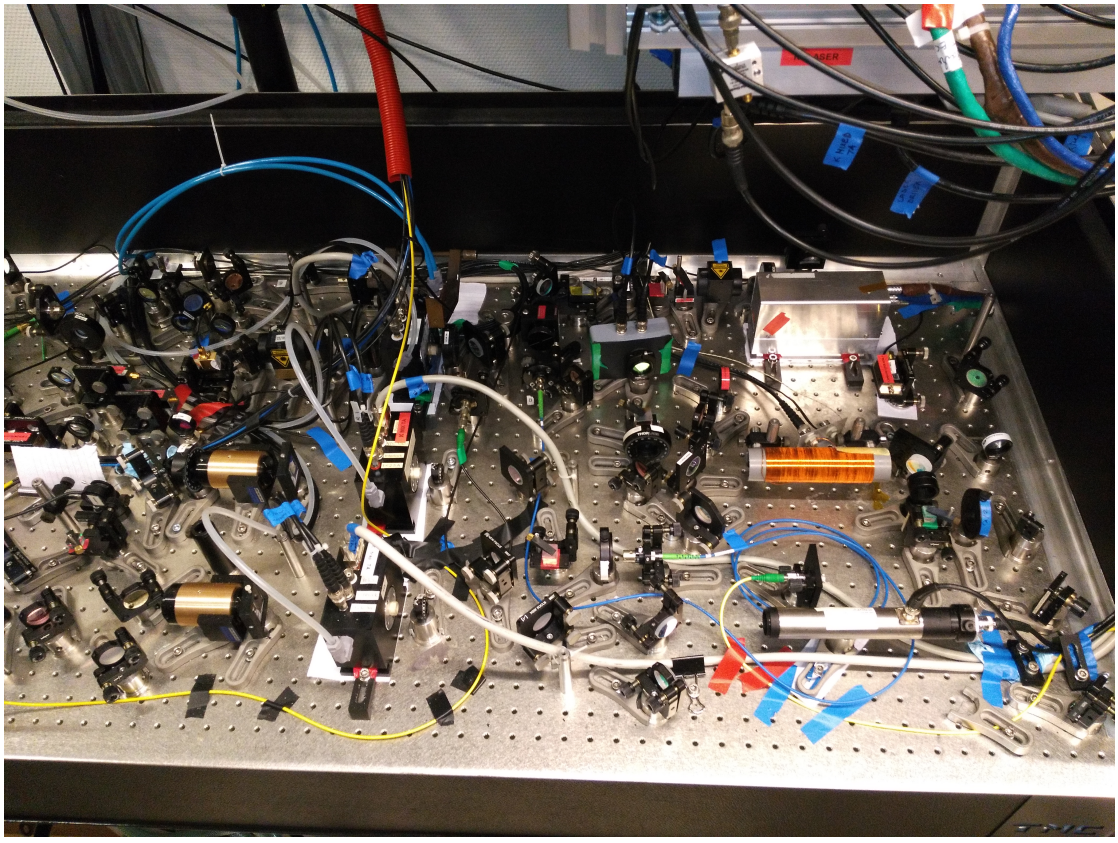


FIGURE 6.7: The optical setup.

6.5 Measurements

Table 6.1 states the optical isolator (I-80-T4-L, before distribution fibre) characteristics.
Table 6.2 states the TA characteristics.
Table 6.3 states the various single pass AOM characteristics.
Table 6.4 states the Brimrose (trap to repump) AOM characteristics.
Table 6.5 states the imaging AOM characteristics without magnetic fields.
Table 6.6 states the optical fibre characteristics.
Table 6.7 states the MOT fibre characteristics.

Transmission	82%
Isolation	32.4 dB

TABLE 6.1: Optical isolator characteristics.

TA	Input Power (mW)	Output Power (mW)	Current (A)
K Mix	12	500	1.9
K Trap	11	480	2.4
K Repump	15	460	1.9

TABLE 6.2: TA characteristics.

AOM (no)	Desired Frequency (MHz)	Actual Frequency (MHz)	Desired Detuning (Γ)	Actual Detuning (Γ)	Diffraction Efficiency (%)	RF Atten--uation (dB)
(0) 2D MOT Trap	76.5	79.9	-3	-2.4	50	7
(1) 2D MOT Repump	83.5	81.6	-2	-2.4	51	7
(3) Push	83.8	83.8	-1.5	-1.7	52	10
(4) 3D MOT Trap	76.5	78.7	-3	-2.6	50	5
(5) 3D MOT Repump	83.5	81.4	-2	-2.4	59	5

TABLE 6.3: Single pass AOM characteristics.

Desired Frequency	-1.2435 GHz
Actual Frequency	-1.2435 GHz
Diffraction Efficiency	7%
RF Power	25 dBm
Max RF Power	30 dBm

TABLE 6.4: Brimrose AOM characteristics.

Desired Resonance Frequency	94.3 MHz
Desired Scanning Detuning Range	2Γ
Desired Scanning Range of Frequency	88.3 MHz -100.3 MHz
Actual Scanning Range of Frequency	96.4 MHz -134.6 MHz
Single Pass Diffraction Efficiency	58%
Double Pass Diffraction Efficiency	25%
RF Attenuation	5 dB

TABLE 6.5: Imaging AOM characteristics.

Fibre name	Coupling Efficiency (%)
Distribution	64
Trap TA	30
Repump TA	45
Push	45
Imaging	48

TABLE 6.6: Optical fibre characteristics.

MOT Type	Trap Efficiency (%)	Repump Efficiency (%)	Repump Waist:Trap Waist
2D	36	59	1
3D	53	48	1.3

TABLE 6.7: MOT fibre characteristics.

Chapter 7

MOT Setup

7.1 Laser Cooling and Trapping

In this section the principle of laser cooling and trapping will be discussed.

7.1.1 Optical Molasses

Optical molasses involves three basic atom-light interaction processes, namely absorption, spontaneous emission and stimulated emission. This is illustrated in figure 7.1. Absorption, occurs when a photon is resonant to a transition of an atom, hence the atom receives a momentum kick in the direction of the photon. Spontaneous emission, occurs when an atom decays from a higher energy state to a lower energy state, leading to emission of a photon in any random direction and correspondingly the atom experiences a recoil. Stimulated emission, occurs when an atom already in an excited state receives a resonant photon and decays into the ground state followed by emission of two photons [3,4].

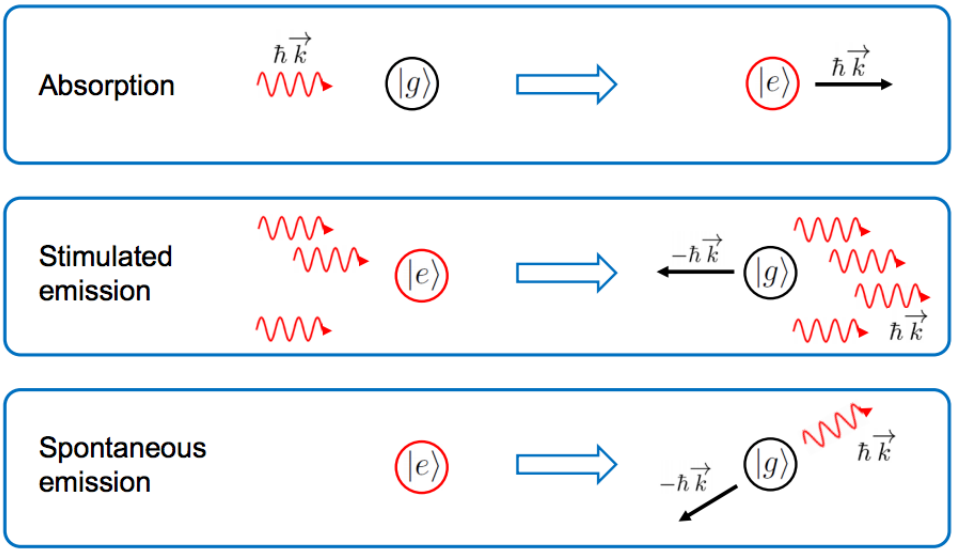


FIGURE 7.1: Atom-light interaction processes [4].

In order to cool the atoms we need to consider these three processes happening in a moving atom. When an atom is moving it will see the frequency of the incoming photon Doppler shifted as described by equation 5.1. To make the photon resonant with the atom the frequency of the photon needs to be shifted to compensate the Doppler effect. Figure 7.2 illustrates the optical molasses beams. These beams are slightly red detuned to the atomic transition used for laser cooling. If an atom happens to be moving against one of the beams, it sees the photons of this beam Doppler shifted to higher frequency.

The photons are now closer to the atomic transition and are more likely absorbed than photons from the other laser beams. Therefore atoms are most likely to absorb photons from beams against which they more or less move, giving them a momentum kick on absorption that slows them down. The term molasses is used as if the atoms were being slowed down by moving through a thick molasses (sugar syrup). Slowing of the atom also leads to it being cooled down. Spontaneous emission leads to momentum kicks in random directions, averaging out after many absorption emission cycles. Energy is removed from the atomic cloud because the emitted photons have in average a higher frequency than the absorbed photons. Entropy is removed from the cloud while still increasing the entropy of the universe because photons are emitted in random directions, increasing the entropy of the light field. By contrast, stimulated emission leads to emission of photons in the same laser mode leaving the entropy and energy unchanged [3,4].

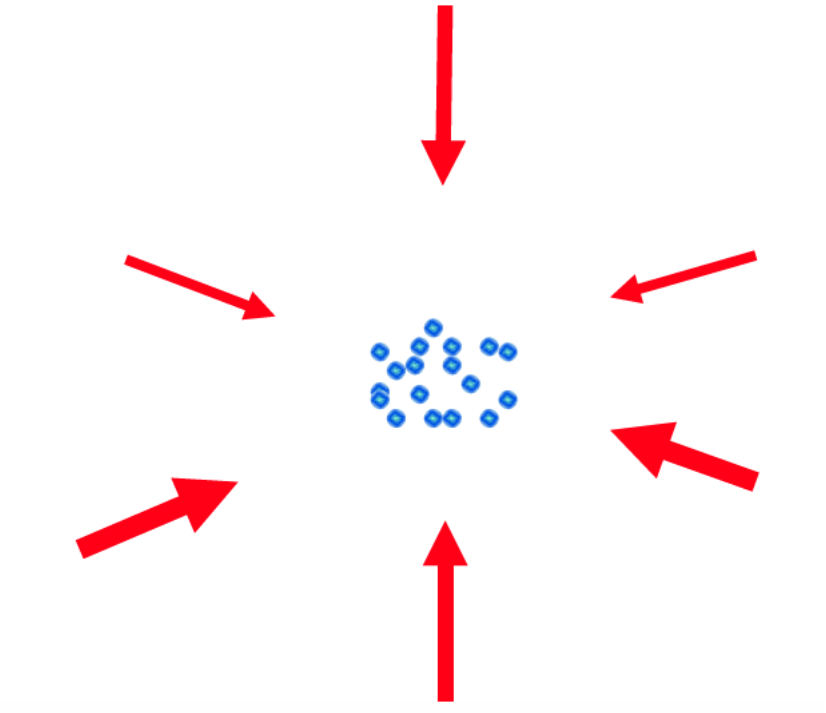


FIGURE 7.2: Optical molasses [4].

7.1.2 Magneto-Optical Trap

The optical molasses only cools down the atoms but cannot concentrate them to one spatial location. For that magnetic fields and circularly polarized molasses beams are required. This is illustrated in figure 7.3. The atoms are concentrated at the centre of the quadrupole magnetic field (B), where B is zero (figure 7.4). A simplified picture of the atom will be considered in the following, with a J=0 ground state and a J=1 excited state. The excited state will split into three non-degenerate magnetic states ($m_J = 0, -1, 1$) because of the Zeeman Effect. This is illustrated in figure 7.5. Next, a quantisation axis needs to be chosen to explain the MOT, for example the x-axis. If the B-field is parallel to the quantisation axis then RHCP (green arrow) will drive $\Delta m_J = 1$ transitions and LHCP (blue arrow) will drive $\Delta m_J = -1$ transitions. Next, considering a situation in which an atom is at B=0 G and starts drifting to the right, initially the red detuned laser beams will be out of resonance but the magnetic field starts increasing and $m_J = -1$

gets lowered in energy and at a particular point (shown by the right red arrow) the atom is in resonance, thus driving the $\Delta m_J = -1$ transition by absorbing a photon and experiencing a recoil momentum, bringing the atom back to the centre. Similarly the $\Delta m_J = 1$ transition is driven when the atom moves to the left, and it is pushed back to the centre. Thus, along with the molasses mechanism the atoms are simultaneously cooled and trapped at a single spatial location [3,4].

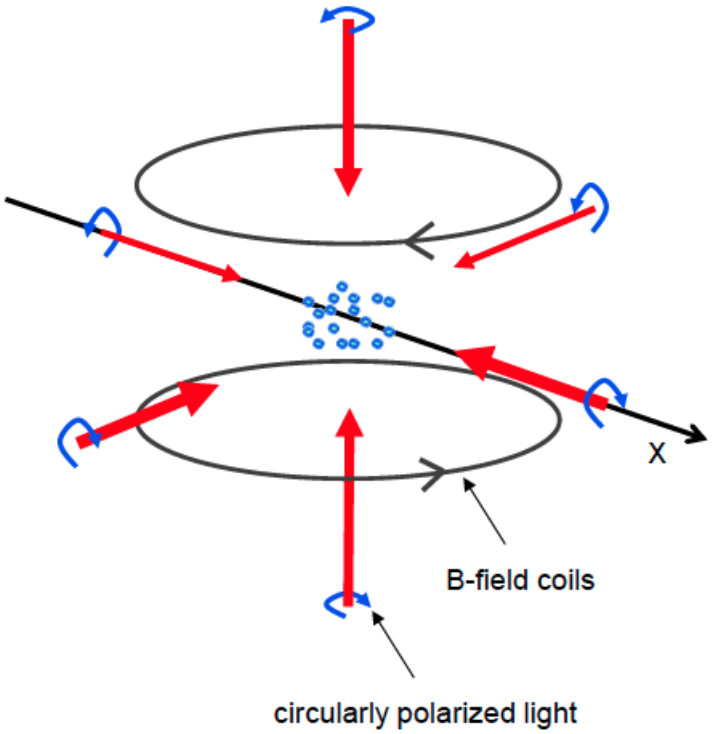


FIGURE 7.3: Magneto-optical Trap [4].

7.2 Vacuum System

The vacuum system was originally built in 2004 [1]. The vacuum system is divided into three connected chambers (A,B,C), see figure 7.6 [1,2]. A is the potassium source chamber, B is the main chamber for a dual species 3D MOT of potassium and lithium, C is the lithium 2D-MOT chamber. There are two ion pumps in chambers B and C. The ion pump in chamber C can be disconnected from the one in chamber B using a valve, but currently it is connected. At the moment only chamber A and B are used, and the optics around them was built in 2015 by Benjamin Pasquiou [2]. The imaging optics was newly installed.

With reference to figure 7.6, chamber A houses a potassium 2D MOT (b) and is a glass cell from Technical Glass Inc. It has four way cross optical quality windows (diameter=30 mm), for the two pairs of 2D MOT beams [1]. On the left side of (b) there is a fifth optical quality window which is used for the push beam. It can also be used for axial cooling [1]. On the right side of the window a 13 mm glass tube is connected with a T-piece to the ampule (a), where potassium is stored. KCl enriched to an abundance of 6% ^{40}K purchased from Trace Science International and distilled into a break-seal ampule by Technical Glass Inc. have been used as a source of potassium [1]. On the right side of (b) is the differential pumping tube, which connects to the ultra-high vacuum (UHV) system (B). This differential pumping tube has 23 mm length and

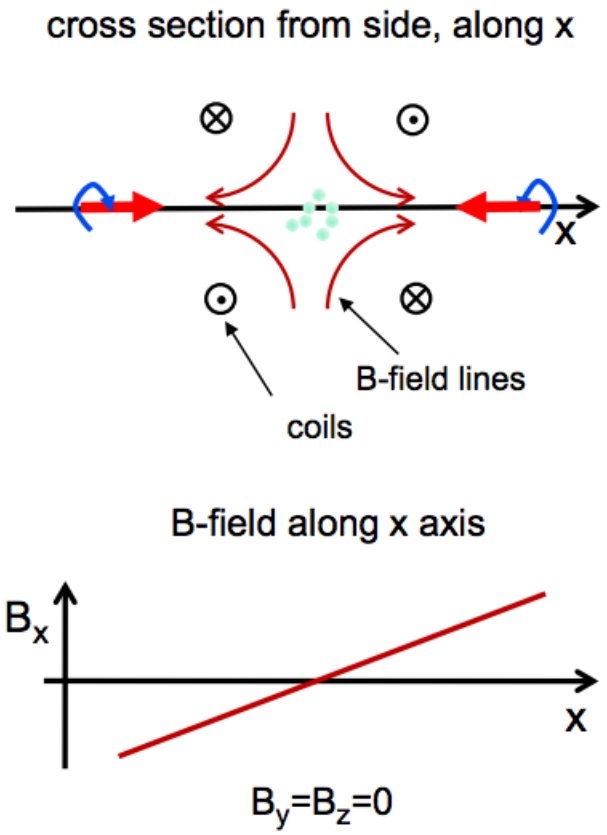


FIGURE 7.4: Quadrupole magnetic field [4].

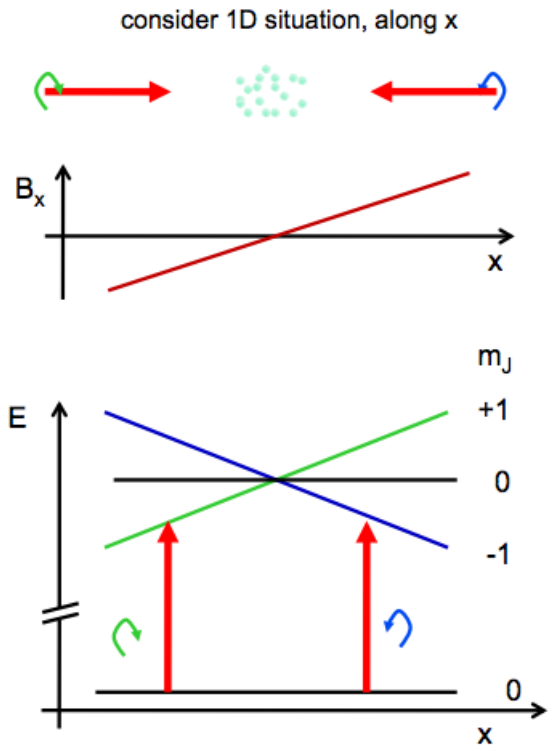


FIGURE 7.5: Splitting of magnetic states in a MOT [4].

2 mm diameter. A gold mirror having a 2 mm orifice at its centre is placed at a distance

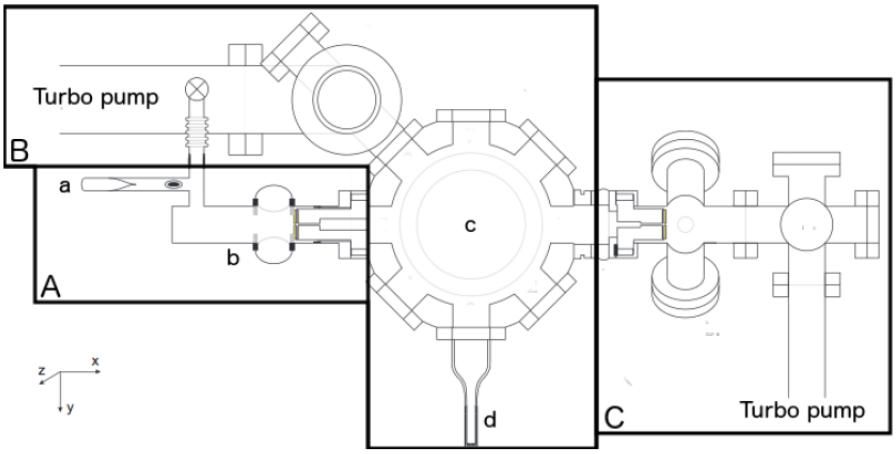


FIGURE 7.6: Schematic of the vacuum system [2].

of 1 mm from the differential pumping tube. This mirror can be used for reflecting a probe beam or for a 1D optical molasses beam [1]. Chamber B has seven optical quality windows, six of them are used for the 3D MOT beams (c). The seventh one is used for transporting the MOT into the science cell (d). The science cell can be used for having good optical access to the atomic cloud and for being able to add strong electromagnets required for polarizing the cloud [2,14]. Currently, the UHV chamber MOT is imaged using this cell as viewport.

The chambers A and B can be heated up to 65°C by wrapping the heating bands around them followed by thermal isolation using aluminium foil. The heating bands are powered by appropriate power supplies. Be cautious to not short-circuit the heating band or connect it to the table (ground) and electrocute your labmates! (they can be very itchy too!). The temperatures are monitored using K-type thermocouples (up to 1250°C) with an error of 0.4%, which can be read on the computer [2].

During the project, some of the heating bands had to be replaced, power supplies had to be re-arranged and the appropriate values of temperature and corresponding voltages was measured. The ambient temperature during the measurements was 22°C.They are stated in Table 7.1 as follows:

Chamber	Temperature (°C)	Voltage (V)	Resistance (Ω)
2D MOT	63	32	100
Differential Pumping	64	34.8	86
Push Beam Window	64	1.5	5
Ampule	50	13.5	85
Glass tube on side of 2D MOT	64	23.2	100

TABLE 7.1: MOT chamber heating bands measurements.

7.3 Optical Setup

7.3.1 2D MOT

A 2D MOT is used for loading a high flux of atoms into the the 3D MOT. This prevents contamination of the UHV of 3D MOT with the hot potassium gas, otherwise which

would have directly been loaded from the ampule.

The 2D MOT requires a 2D quadrupole field created by four permanent magnets [2] and two pairs of counter-propagating red- detuned laser beams. The laser beams are made counter- propagating by retro-reflecting them. The 2D MOT setup is illustrated in figure 7.7.

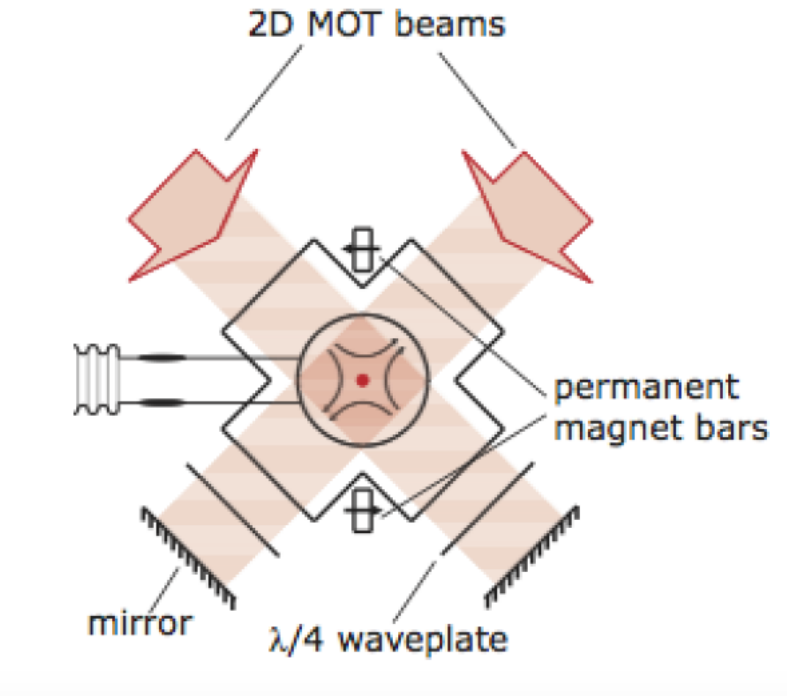


FIGURE 7.7: 2D MOT setup [1].

7.3.2 3D MOT

The 3D MOT setup comprises of six independent beams. The quadrupole magnetic field is created by two electric coils in anti-Helmholtz configuration (current running in counter-sense with respect to each other). The vertical beams have a smaller waist as the horizontal beams because of difference in window size. Figure 7.8 shows the MOT setup.

7.4 Fluorescence Imaging

For characterizing the number of atoms in a MOT it needs to be imaged. This can be done by estimating the number of photons (fluorescence) scattered from the MOT. An Andor CCD camera is used for capturing the fluorescence. The camera was calibrated using an LED, to precisely determine how many photons correspond to each count of the camera. The setup is illustrated in figure 7.9.

Our next step is to calculate the number of photons scattered by a single atom. For this the absorption cross-section (σ) needs to be calculated, given by

$$\sigma = \frac{3\lambda^2}{2\pi} \frac{1}{1 + (2\delta/\Gamma)^2}, \tag{7.1}$$

where δ is the detuning of the MOT beams from the trap transition and σ multiplied by the number of photons scattered per unit area, gives the number of photons scattered

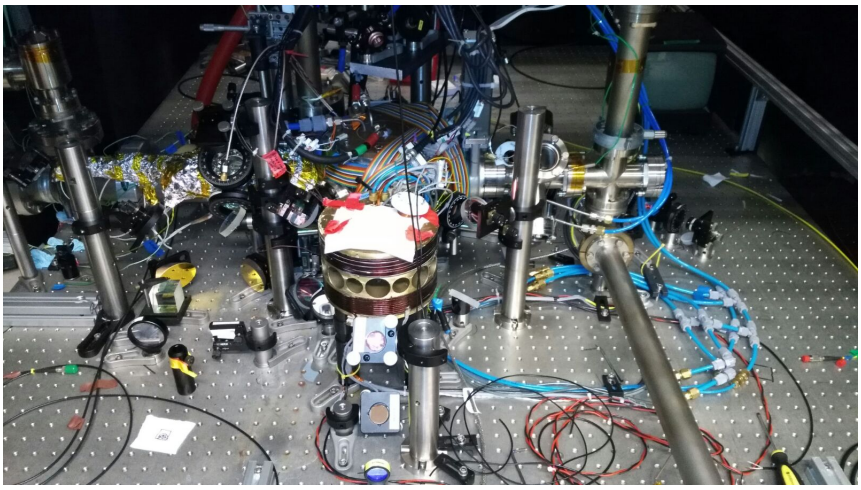


FIGURE 7.8: Vacuum chamber surrounded by magnets and, MOT and imaging optics.

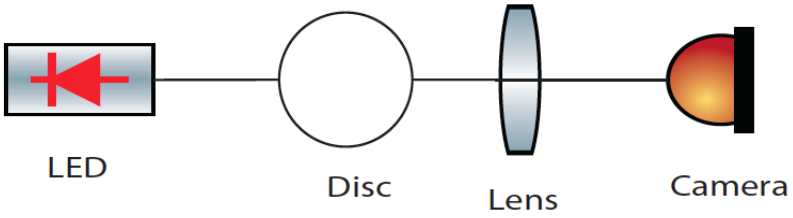


FIGURE 7.9: Camera calibration setup.

per unit atom. The total number of scattered photons divided by number of photons scattered per unit atom gives the number of atoms in the MOT.

7.4.1 Calibrations

Dish Diameter	25 mm
LED Power	3.75 μW
Pixel Number (N_{pixel})	1004×1002
Pixel Area (A_{pixel})	$8 \times 8 \times 10^{-12}$ m^2
Exposure Time (ET)	10 ms
LED Wavelength	650 nm
Gain	1
Quantum Efficiency	0.63
Count per pixel	5472.38

TABLE 7.2: Measurements for calibrating Andor camera.

Table 7.2 gives the experimentally measured values for calibrating the camera. The intensity of light on LED Dish (I_{dish}), where $I_{\text{dish}} = \frac{LED\ Power}{Dish\ Area}$ is calculated to be 4.9×10^{-4} W/m^2. Next, the total energy of the photons (E_{total}) incident on the camera is given by

$$E_{\text{total}} = I_{\text{dish}} \times N_{\text{pixel}} \times A_{\text{pixel}} \times ET, \tag{7.2}$$

which is calculated to be 4.9×10^{-9} J. Next, the total number of photons (N_{photon}) incident on the camera can be calculated using

$$N_{\text{photon}} = \frac{E_{\text{total}}}{E_{\text{photon}}}, \tag{7.3}$$

where E_{photon} equals to, 3.1×10^{-19} J. After calculation, $N_{\text{photon}} = 1.6 \times 10^{10}$. The final step is to calculate the corresponding number of photons for one count of the camera (count to photon), which is given by

$$\text{count to photon} = \frac{N_{\text{photon}} \times QE \times Gain}{N_{\text{pixel}} \times \text{countperpixel}}. \tag{7.4}$$

After calculation, one count corresponds to $1.8 \sim 2$ photons.

7.5 Absorption Imaging

Absorption imaging is a powerful and robust technique to give information about the MOT cloud. After the atoms are trapped in the MOT, the trap is switched off and the cloud of atoms expands and falls down under gravity. The atoms expand more if they are faster i.e. hotter. After a certain time (20 ms or so) a probe beam resonant to the strong atomic transition also used for the MOT is shone on the atoms. The atoms scatter photons out of the laser beam and cast a shadow. The intensity profile of the laser beam is imaged using a lens onto a CCD camera. In addition, an image without the atoms is recorded by the camera. Finally, the image with atoms is normalized pixel-by-pixel by the image without atoms and the logarithm of the normalized picture gives the density of the cloud integrated along the direction of the probe. Figure 7.10 illustrates the absorption imaging procedure [4].

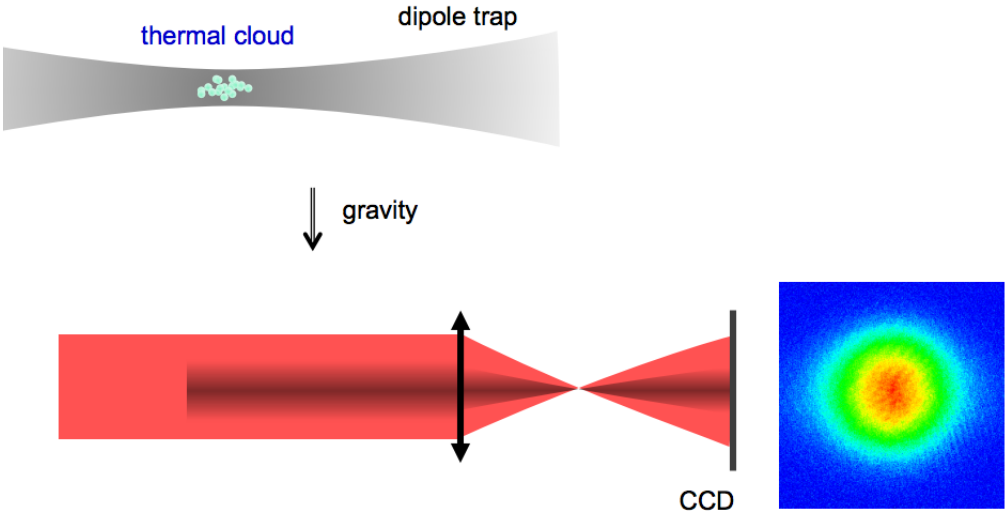


FIGURE 7.10: Absorption imaging [4].

7.5.1 Mathematical Description

The change in intensity with distance is given by the Absorption or Beer's Law, which is

$$\frac{dI}{dz} = -\sigma_{\text{abs}} n I, \tag{7.5}$$

where n is the atom density and I is the intensity. The on-resonance absorption parameter (σ_{abs}) can be calculated using equation 7.1. The atom density ($n_{\text{int}}(x, y)$) is given by

$$n_{\text{int}}(x, y) = \int n(x, y, z) dz = -\frac{1}{\sigma_{\text{abs}}} ln \left(\frac{I_{\text{end}}(x, y)}{I_{\circ}(x, y)} \right). \tag{7.6}$$

Figure 7.11 illustrates equation 7.6 [4].

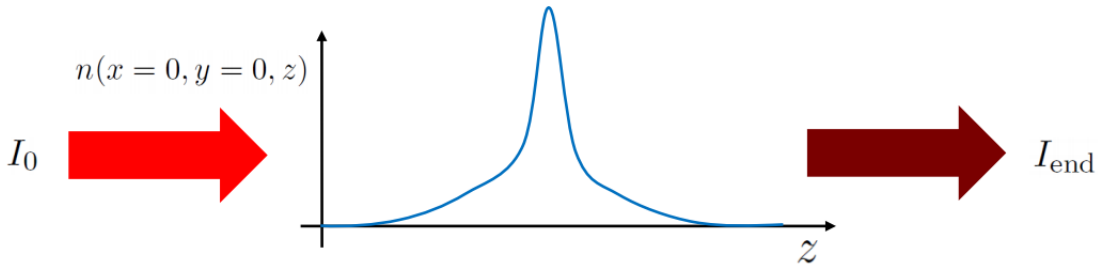


FIGURE 7.11: Beer's law [4].

7.5.2 Optical setup

A dual imaging setup has been designed for both fluorescence and absorption imaging, see figure 7.12. The waist of the beam after the imaging fibre's output coupler is 0.6 mm. The imaging beam's waist is magnified by a factor 10 using a telescope. The waist has been chosen such that the intensity of the probe beam is enough to saturate the atoms. The waist should be chosen to cover the area of interest for imaging. It might be limited by power constraints. After the 3D MOT, the magnification of the telescope is 0.5, so that the whole 3D MOT can be imaged, without being clipped. The lens cannot be approached closer than 13 cm to the atoms. Two inch optics is recommended, to capture more fluorescence photons and make best use of the available numerical aperture. The typical diameter of a potassium 3D MOT is around 3.5 mm [1].

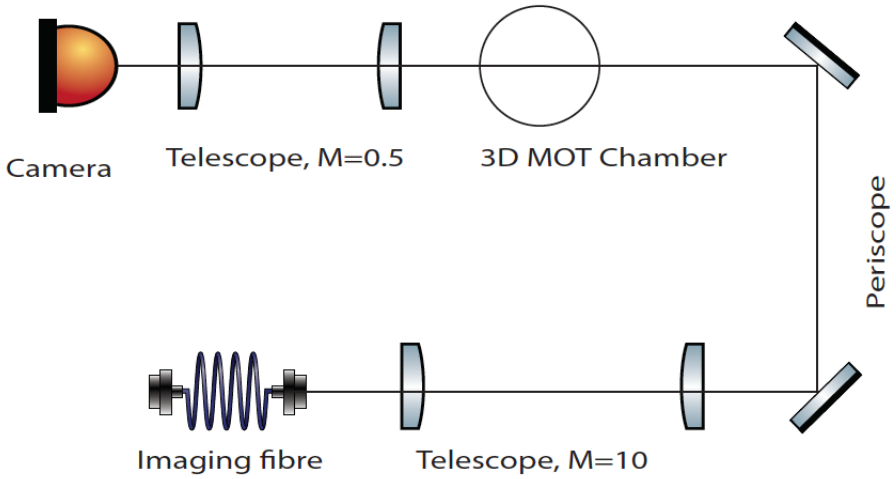


FIGURE 7.12: Imaging setup.

Chapter 8

Summary and Outlook

8.1 Summary

During the course of this thesis, firstly, the computer control system for the experiment was implemented and calibrated. Secondly, the master laser was repaired, after condensation on the diffraction grating and realigned. Thirdly, the laser lock setup was rebuilt with improved stability ($\sim$a day) and experimental results were better understood by making a comparison with simulations. Fourthly, the amplifier optical setup was modified and rebuilt, with improved stabilization of output power after the tapered amplifiers and optical fibres. Fifthly, the absorption imaging setup was built and the Andor camera was calibrated.

8.2 Outlook

In future with the improved setup, the MOT should be measured with better stability and precision. After obtaining a MOT, the final steps in order to obtain a quantum degenerate gas is loading the atoms into an Optical-Dipole trap (ODT) and performing evaporative cooling. The hottest atoms evaporate from the dipole trap, leaving behind colder atoms that thermalize by elastic collisions to a lower temperature. At the lower temperature, less atoms have a high enough energy to escape the trap. In order to keep evaporation going at a sufficient rate, the dipole potential is lowered over a few seconds by reducing the dipole trap laser power [4].

While cooling the atoms, one is limited by the natural linewidth of the atom (Doppler temperature). But by varying the polarization of the laser beam in space, it is possible to optically pump the atoms into two different grounds states, driving σ^+ and σ^- transitions alternately. This can be considered as the atom losing kinetic energy every time it needs to climb a hill. Thus, cooling down the atoms to sub-doppler temperatures, known as Sisyphus cooling [3,4].

Sub-doppler cooling [3,4] on the D2 transition leads to reduced atom numbers of the MOT, because the $^2\mathrm{P}_{3/2}$ excited state of ^{40}K has a narrow, inverted hyperfine level structure, which leads to inefficient optical pumping[25]. Hence, gray molasses cooling beams on the D1 transition can be used for reaching sub-doppler temperatures with decent atom numbers of the MOT [25].

Once a quantum degenerate gas of fermions is obtained, our group plans to study itinerant ferromagnetism in one dimension [7]. For engineering these magnetic interactions, we plan to make use of an exceptional situation occurring in fermionic potassium, i.e. overlapping p- and s-wave Feshbach resonances [5]. These studies can enhance our understanding of strongly correlated systems [7].

Bibliography

[1] Tobias Tiecke, Feshbach Resonances in ultracold mixtures of the fermionic quantum gases of ^{6}Li and ^{40}K, PhDThesis, University of Amsterdam (2009).

[2] Wouter Meinster, The creation of a potassium-40 magneto-optical trap, Master Thesis , University of Amsterdam (2015).

[3] H. J. Metcalf and P. van der Straten, *Laser Cooling and Trapping* (Springer-Verlag, New York, 1999).

[4] Florian Schreck, *Lectures on Bose-Einstein Condensates*, University of Amsterdam (Autumn 2014).

[5] Florian Schreck, *Lectures on Quantum Simulation*, University of Amsterdam (Spring 2015).

[6] J.H.Fewkes and John Yarwood, *Atomic Physics* ,Vol. II (Oxford Univ. Press, 1991).

[7] Jiang *et al.*, Phys. Rev. A **94**, 011601 (2016).

[8] T.G. Tiecke, *Properties of Potassium.*

[9] Florian Schreck, *Manual of the ultracold atom experiment control system "CONTROL"* (2011).

[10] Wenxian Hong , *Design and Characterization of a Littrow Configuration External Cavity Diode Laser.*

[11] C. Wieman and T.W. Hänsch, Phys. Rev. Lett. 36, 1170 (1976).

[12] Maarten Mooij, Laser Lock for Laser Cooling and Trapping of Potassium-40, Bachelor Thesis, University of Amsterdam (2015).

[13] An Introduction to the New Focus TA-7600 VAMP Tapered Amplifier.

[14] Antje Ludewig, Feshbach Resonances in ^{40}K, PhD Thesis, University of Amsterdam (2012).

[15] Richard P. Feynman, International Journal of Theoretical Physics, Vol 21, Nos. 6/7, (1982).

[16] www.thepistrophy.com

[17] http://webpages.ursinus.edu/lriley/ref/circuits/node4.html

[18] https://en.wikipedia.org/wiki/Periodic_table

[19] http://www.electrical4u.com/what-is-servo-motor

[20] http://www.moglabs.com

[21] http://www.elent-a.net

[22] https://en.wikipedia.org/wiki/Optical_fiber

[23] https://alker.co.uk/product/panda-2

[24] SM 15-200 D Manual, Schulz Electronic (May 2008).

[25] D. R. Fernandes *et al*, Europhys. Lett. 100, 63001 (2012).

Appendix A

Computer Code

```
void SetFrequencyK3DMOTTrapAOM(double Frequency) {
    long double aVoltage=-9.08493+(0.14987*Frequency)+(0.00184*pow(Frequency,2))-(0.0000102261*pow(Frequency,3));
    long double Voltage=aVoltage/1.3019726858877086494688922610015; //This output card has been modified to produce -13.1 to +13.1 V.
    Output->AnalogOutScaled(BASE_ANA_B + 4,Frequency,Voltage);//The Output->AnalogOutScaled assumes -10V to +10V. We need to convert here.
}

void SetFrequencyK3DMOTRepumpAOM(double Frequency) {
    long double aVoltage=-10.46556+(0.24405*Frequency)-(0.0000310379*pow(Frequency,2));
    long double Voltage=aVoltage/1.3035230352303523035230352303523; //This output card has been modified to produce -13.1 to +13.1 V.
    Output->AnalogOutScaled(BASE_ANA_B + 5,Frequency,Voltage); //The Output->AnalogOutScaled assumes -10V to +10V. We need to convert here.
}
```

FIGURE A.1: Excerpt of the VCO calibration code.

```
const unsigned int VCANr=1000;
CStepwiseLinearCalibration *CalibVoltage[VCANr];
void LoadVCACalibration(int VCANr) {
    if (VCANr==NotConnected) return;
    CString buf;
    buf.Format("C:\\K\\ControlK\\Calibrations\\CalibVCA%i.dat",VCANr);
    CalibVoltage[VCANr]=new CStepwiseLinearCalibration(buf,100,false);
}
```

```
void SetAttenuationK2DMOTTrapAOM(double Attenuation)
{
    if (Output->InScaledOutStoreMode())
    {
        LoadVCACalibration(0);
    }
    Output->RangeCheck(Attenuation,3.85,68.85,"SetAttenuationK2DMOTTrapAOM");
    if(CalibVoltage[0])
        Output->AnalogOutScaled(BASE_ANA_F+0,Attenuation,CalibVoltage[0]->ConvertXToY(Attenuation));
}

void SetAttenuationK2DMOTRepumpAOM(double Attenuation) {
    if (Output->InScaledOutStoreMode())
    {
        LoadVCACalibration(1);
    }
    Output->RangeCheck(Attenuation,3,68,"SetAttenuationK2DMOTRepumpAOM");
    if(CalibVoltage[1]) {
        Output->AnalogOutScaled(BASE_ANA_F+1,Attenuation,CalibVoltage[1]->ConvertXToY(Attenuation));
    }
}
```

FIGURE A.2: Excerpt of the VCA calibration code.

```
//Magnetic Coils....Analog Outputs
void SetK3DMOTCoilsCurrent(double Current) {
    Output->RangeCheck(Current,0,200,"SetK3DMOTCoilsCurrent");
    double OutVoltage=(0.02546*Current)+0.01084;   //Programming voltage=0.02546*current + 0.01084, see 10.5.2006
    if (OutVoltage>10) OutVoltage=10;
    if (OutVoltage<-0.5) OutVoltage=-0.5;
    Output->AnalogOutScaled(BASE_ANA_D+3,Current,OutVoltage);
}
```

FIGURE A.3: Excerpt of MOT coils programming code.

```
void SwitchCameraTriggerAndor0(bool OnOff) {
    Output->DigitalOutScaled(0,OnOff,OnOff);    // K horizontal
}

const int Switch2DMOTShutterServoSignalChannelNr=1;
void Switch2DMOTShutterServoSignal(bool OnOff) {
    Output->DigitalOutScaled(Switch2DMOTShutterServoSignalChannelNr,OnOff,OnOff);
}

void Switch2DMOTShutter(bool OnOff) {
    PositionServo(Switch2DMOTShutterServoSignalChannelNr,OnOff,/*OnPulseDuration*/1.,/*OffPulseDuration*/2.0 ,/*PulseSequenceDuration*/110,/*smoothly*/false,/*PulseSeparation*/3);
    Output->DigitalOutScaled(HelpDigitalOutStartNumber+Switch2DMOTShutterServoSignalChannelNr,OnOff,!OnOff);
}
```

FIGURE A.4: Computer code for manoeuvring the shutters.